Coordination Chemistry Reviews 254 (2010) 2281–2296

Contents lists available at ScienceDirect

Coordination Chemistry Reviews

journal homepage: www.elsevier.com/locate/ccr

Review

Supramolecular coordination chemistry of aromatic polyoxalamide ligands: A metallosupramolecular approach toward functional magnetic materials

Marie-Claire Dul[a], Emilio Pardo[a,*], Rodrigue Lescouëzec[a], Yves Journaux[a,b,**], Jesús Ferrando-Soria[c], Rafael Ruiz-García[c,d], Joan Cano[c,d], Miguel Julve[c], Francesc Lloret[c,*], Danielle Cangussu[e], Cynthia L.M. Pereira[f], Humberto O. Stumpf[f,*], Jorge Pasán[g], Catalina Ruiz-Pérez[g,*]

[a] *Institut Parisien de Chimie Moléculaire, UPMC Univ Paris 06, Paris, France*
[b] *CNRS, UMR7201, Institut Parisien de Chimie Moléculaire, Paris, France*
[c] *Departament de Química Inorgànica, Instituto de Ciencia Molecular (ICMol), Universitat de València, Paterna, València, Spain*
[d] *Fundació General de la Universitat de València (FGUV), València, Spain*
[e] *Instituto de Química, Universidade Federal de Goiás, Goiânia, Brazil*
[f] *Laboratório de Química de Materiais Moleculares (LQMMol), Departamento de Química (ICEx), Universidade Federal de Minas Gerais, Belo Horizonte, Brazil*
[g] *Laboratorio de Rayos X y Materiales Moleculares, Departamento de Fisica Fundamental II, Universidad de La Laguna, Tenerife, Spain*

Contents

Abbreviations: ACU, antiferromagnetic coupling unit; APOXA, aromatic polyoxalamide; DFT, density functional theory; FCU, ferromagnetic coupling unit; MMW, molecular magnetic wire; MMS, molecular magnetic switch; MOC, metal–organic cluster; MOL, metal–organic ligand; MOP, metal–organic polymer; MOS, metal–organic switch; MOW, metal–organic wire; OFM, open-framework magnet; POL, polytopic organic ligand; Qubit, quantum bit; SCM, single-chain magnet; SMM, single-molecule magnet.

* Corresponding authors.
** Corresponding author at: Institut Parisien de Chimie Moléculaire, UPMC Univ Paris 06, Paris, France. Tel.: +33 1 44 27 55 62; fax: +33 1 44 27 38 41.
E-mail addresses: emilio.pardo@uv.es (E. Pardo), yves.journaux@upmc.fr (Y. Journaux), francisco.lloret@uv.es (F. Lloret), stumpf@qui.ufmg.br (H.O. Stumpf), caruizperez@gmail.com (C. Ruiz-Pérez).

0010-8545/$ – see front matter
doi:10.1016/j.ccr.2010.03.003

ARTICLE INFO

Article history:
Received 21 January 2010
Accepted 8 March 2010
Available online 15 March 2010

Dedicated to the late Professor Olivier Kahn.

Keywords:
Metallosupramolecular chemistry
Metal–organic clusters
Metal–organic polymers
Molecular magnets
Polytopic ligands
Self-assembly

ABSTRACT

The impressive potential of the metallosupramolecular approach in designing new functional magnetic materials constitutes a great scientific challenge for the chemical research community that requires an interdisciplinary collaboration. New fundamental concepts and future applications in nanoscience and nanotechnology will emerge from the study of magnetism as a supramolecular function in metallosupramolecular chemistry. Our recent work on the rich supramolecular coordination chemistry of a novel family of aromatic polyoxalamide (APOXA) ligands with first-row transition metal ions has allowed us to move one step further in the rational design of metallosupramolecular assemblies of increasing structural and magnetic complexity. Thus, we have taken advantage of the new developments of metallosupramolecular chemistry and, in particular, the molecular-programmed self-assembly methods that exploit the coordination preferences of paramagnetic metal ions and suitable designed polytopic ligands. The resulting self-assembled di- and trinuclear metallacyclic complexes with APOXA ligands, either metallacyclophanes or metallacryptands, are indeed ideal model systems for the study of the electron exchange mechanism between paramagnetic metal centers through extended π-conjugated aromatic bridges. So, the influence of different factors such as the topology and conformation of the bridging ligand or the electronic configuration and magnetic anisotropy of the metal ion have been investigated in a systematic way. These oligonuclear metallacyclic complexes can be important in the development of a new class of molecular magnetic devices, such as molecular magnetic wires (MMWs) and switches (MMSs), which are major goals in the field of molecular electronics and spintronics. On the other hand, because of their metal binding capacity through the outer carbonyl-oxygen atoms of the oxamato groups, they can further be used as ligands, referred to as metal–organic ligands (MOLs), toward either coordinatively unsaturated metal complexes or fully solvated metal ions. This well-known "complex-as-ligand" approach affords a wide variety of high-nuclearity metal–organic clusters (MOCs) and high-dimensionality metal–organic polymers (MOPs). The judicious choice of the oligonuclear MOL, ranging from mono- to di- and trinuclear species, has allowed us to control the overall structure and magnetic properties of the final oxamato-bridged multidimensional (*nD*, *n* = 0–3) MOCs and MOPs. The intercrossing between short- (nanoscopic) and long-range (macroscopic) magnetic behavior has been investigated in this unique family of oxamato-bridged metallosupramolecular magnetic materials expanding the examples of low-dimensional, single-molecule (SMMs) and single-chain (SCMs) magnets and high-dimensional, open-framework magnets (OFMs), which are brand-new targets in the field of molecular magnetism and materials science.

1. Introduction and background: metallosupramolecular magnetic materials

The design and synthesis of molecules that are capable of spontaneously associating into large, well-defined assemblies (supermolecules) joined by noncovalent intermolecular interactions remain one of the foremost challenges in supramolecular chemistry [1]. Nature offers countless examples of self-assembling processes that may inspire the work of the synthetic chemist aiming at creating chemical analogues of complex natural structures such as the viral coats and the ribosomes which are made up of many protein and nucleic acid subunits, respectively. Hydrogen and coordinative bonds represent two main synthetic tools in self-assembling chemical systems, referred to as organic [2] and metal–organic [3] approaches, respectively. These two approaches of supramolecular synthesis exploit the specificity and directionality of these relatively weak noncovalent interactions, either hydrogen- or coordination bonds, over strong covalent bonds.

The spectacular development of supramolecular coordination chemistry (termed metallosupramolecular chemistry) in the late 1980s and 1990s has set up the guiding principles for the self-assembly of well-defined multimetallic coordination architectures of increasing structural complexity that are based on metal–ligand interactions [3]. Discrete zero-dimensional (0D) coordination clusters [4], as well as infinite, one- (1D), two- (2D), or three-dimensional (3D) coordination polymers [5], referred to as metal–organic clusters (MOCs) and metal–organic polymers (MOPs) respectively, are included in this category (Fig. 1).

At the beginning of this new century, the introduction of functionality into these metallosupramolecular compounds has become one of the aims of a large number of research groups working in metallosupramolecular chemistry [6,7]. They take advantage from the chemical reactivity (redox or photochemical) and electronic properties (magnetic or optical) of the metal ions and eventually the organic ligands, as well as from the particular level of organization created by the metal–ligand coordinative interaction. In general, the unique properties exhibited by these hybrid inorganic–organic systems are not the sum of those from the individual components but they derive from the cooperative interactions between the metal ions through the organic bridging ligands. The study of the supramolecular structure–function correlations will then orientate the rational design and synthesis of self-assembled supramolecular functional materials. They display interesting physicochemical properties that could be exploited in supramolecular recognition and catalysis [6] and supramolecular photo-, electro-, and magnetochemistry [7] (Fig. 1).

In pursuing metallosupramolecular magnetic materials [8], ligand design is crucial both to organize the paramagnetic metal ions in a desired topology and to efficiently transmit electron exchange interactions between the metal ions in a controlled manner [9,10]. This basic principle is impressively supported by the work on the magnetic properties of oxamato-bridged multimetallic coordination compounds which was initiated by Kahn and coworkers in the late 1980s and then extended to the oxamidato-bridged analogues by Journaux and Lloret in the late 1990s [11,12]. In this pioneering work, aliphatic or aromatic group-substituted bis(oxamato)- [11] and related bis(oxamidato)-copper(II) complexes [12] were used as ligands, referred to as metal–organic ligands (MOLs), toward other metal ions for the preparation of both MOCs and MOPs. Such oxalamide-based metallosupramolecular species whose dimensionality can be tuned will be of great impor-

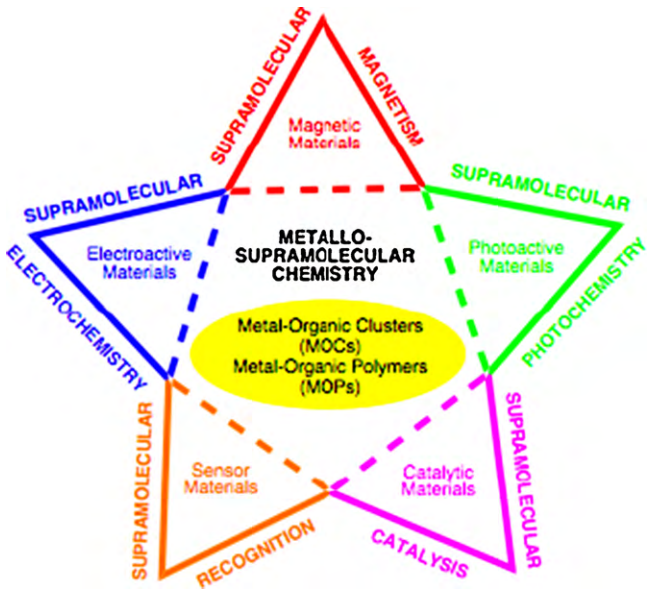

Fig. 1. Relationships between metallosupramolecular chemistry and other areas of supramolecular chemistry and materials chemistry.

tance in the rational design of molecular magnets [13]. Among the range of device-oriented goals based on molecular magnets, the storage and processing of information in quantum computation are particularly relevant. In fact, the incorporation of localized unpaired electrons and the corresponding spin-relaxation or spin-ordering phenomena into molecules and supramolecular materials provide the basis for a wealth of fascinating applications in the rapidly developing new fields of molecular electronics and spintronics. This "bottom-up" metallosupramolecular approach appears as an advantageous alternative to the classical "top-down" one to functional magnetic materials.

Inspired by this work, we have further extended this well-recognized "complex-as-ligand" approach by using oligonuclear complexes of late first-row transition metal ions, from mono- to di- and trinuclear species, with a novel family of aromatic-substituted mono-, bis-, and tris(oxalamide) ligands as MOLs. The present review expands an earlier one on this same subject [12c] by quoting our recent results in this area which have a bearing on the molecular electronics theme of this special issue. The potentialities of the metallosupramolecular design strategy will first be outlined. Then, the main observations concerning the hydrogen bond-directed and the metal-mediated self-assembly of aromatic polyoxalamide ligands will be highlighted. A particular attention will be paid to the structure and magnetism of the oligonuclear MOLs and the resultant MOCs and MOPs of variable nuclearity and dimensionality, respectively. Further, the potential applications of some of these metallosupramolecular magnetic materials in the field of molecular electronics and spintronics will be briefly mentioned.

2. Metallosupramolecular design strategy: molecular-programmed self-assembly of organic and metal–organic ligands

The design and synthesis of polytopic organic ligands (POLs) which are able to self-assemble spontaneously with paramagnetic metal ions through metal–ligand interactions rendering more complex exchange-coupled, polymetallic aggregates with prefixed nuclearity, dimensionality, and topology are major goals in the field of metallosupramolecular magnetic materials. Our strategy in this field has focused on the *N*-phenyloxamate (**1a**), *N,N′*-1,3-phenylenebis(oxamate) (**2a**), *N,N′*-1,4-phenylenebis(oxamate) (**2a′**), *N,N′,N″*-1,3,5-benzenetriyltris(oxamate) (**3a**), and oxamidate-*N,N′*-bis(3-phenyloxamate) (**4a**) ligands together with their polymethyl-substituted analogues (Fig. 2). These homo- and heterotopic, aromatic polyoxalamide (APOXA) ligands consist of a more or less rigid polymethyl-substituted benzene scaffold having multiple oxamato and/or oxamidato donor groups with

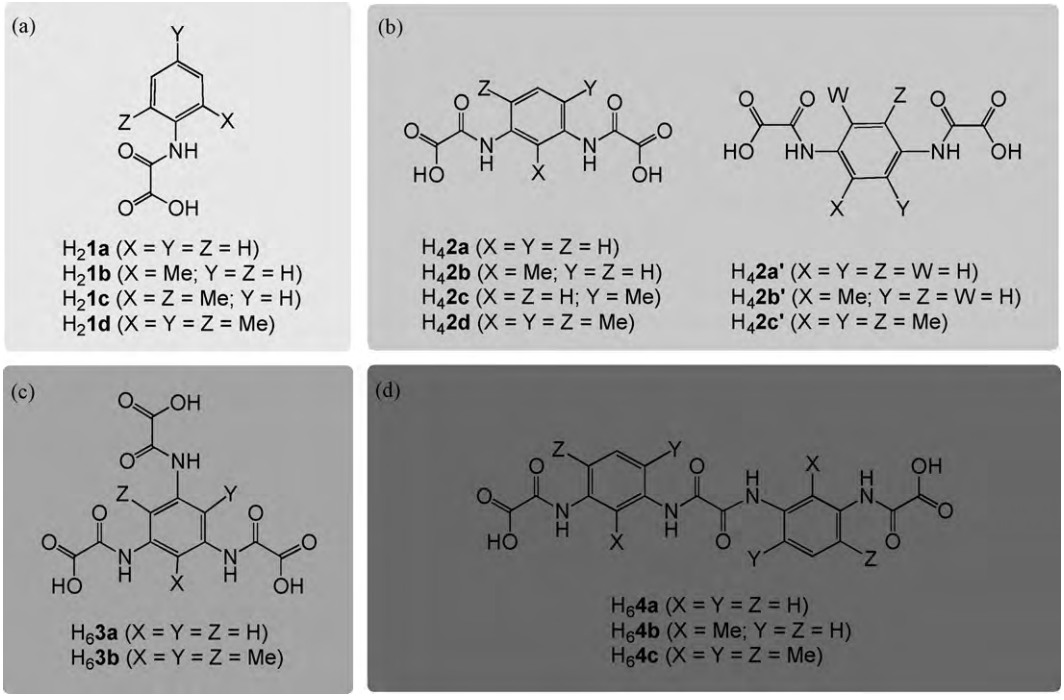

Fig. 2. APOXA ligands of different coordination modes: (a) mononucleating ligands, (b) dinucleating ligands, (c) triangular and (d) linear trinucleating ligands.

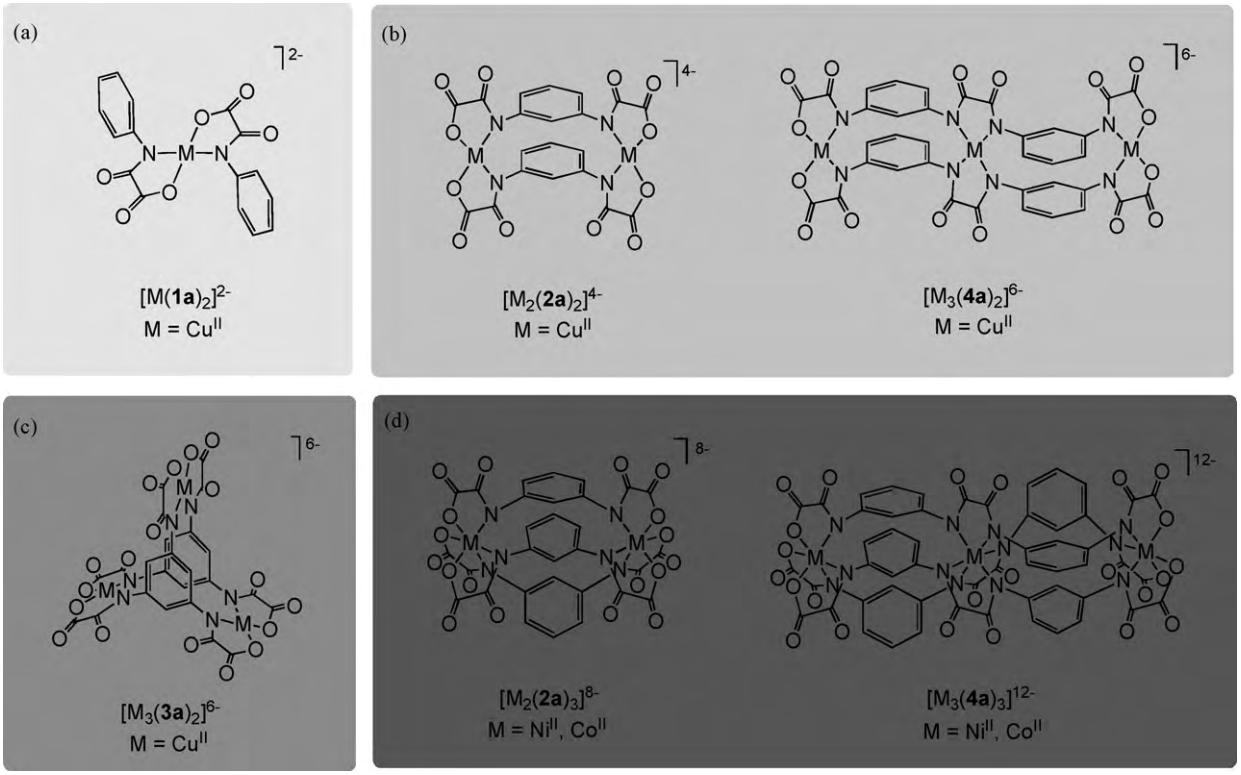

Fig. 3. Self-assembling oxalamide-based MOLs with late 3d divalent metal ions of various preferred coordination geometries: (a) double-stranded mononuclear square-planar copper(II) complexes, (b) linear, double-stranded di- and trinuclear square-planar copper(II) complexes, (c) triangular, cage-like trinuclear square-planar copper(II) complexes, and (d) linear, triple-stranded di- and trinuclear octahedral nickel(II) and cobalt(II) complexes.

different substitution patterns. Depending on the number of oxalamide metal binding sites, from one to two and three, they can be classified as ligands of the first- (L = **1a**–**d**), second- (L = **2a**–**d** and **2a**′–**c**′), and third-generation (L = **3a**–**b** and **4a**–**c**), respectively. The great versatility of this new family of APOXA ligands lies on the variety of coordination modes of each class.

A variety of complex metallosupramolecular assemblies with predictable structural and magnetic properties can be rationally designed and synthesized from the combination of each class of APOXA ligands with late and middle 3d divalent metal ions. In fact, APOXA ligands offer a kind of double programming according to the terminology of metallosupramolecular chemistry.

2.1. Molecular-programmed self-assembly of polytopic organic ligands

The first level of ligand programming in APOXAs allows the coordination of these POLs to the M^{II} ions (M = Cu, Ni, and Co) through the amidate-nitrogen and carboxylate-oxygen donor atoms of the oxamato and/or oxamidato groups. This molecular-programmed self-assembly approach allows the rational preparation of linear double- and triple-stranded as well as triangular cage-like oligonuclear complexes, from mono- to di- and trinuclear species, depending on the molecular symmetry and coordination mode (topicity) of the POLs and the preferred coordination geometry of the metal ions (Fig. 3).

2.2. Molecular-programmed self-assembly of metal–organic ligands

The second level of ligand programming in APOXAs resides precisely on the free carbonyl-oxygen donor atoms of the oxamato and/or oxamidato groups which allow these self-assembled mono-, di-, and trinuclear, square-planar or octahedral complexes to be used as MOLs toward other M'^{II} ions (M′ = Cu, Ni, Co, and Mn). This molecular-programmed self-assembly approach allows the rational preparation of either MOCs or MOPs of varying nuclearity, topology, and dimensionality, depending on the coordination mode of the MOLs and on the presence of blocking ligands in the coordination sphere of the coordinated metal ions that would preclude the polymerization (Fig. 4).

3. Polytopic organic ligands (POLs): from molecules to higher dimensionality hydrogen-bonded supramolecular solids

The H_nEt_nL POLs (L = **1a**–**d**, **2a**–**d**, **2a**′–**c**′, and **3a**–**b**; n = 1–3) were synthesized in the form of the polyethyl ester acid derivatives from the straightforward reaction of the corresponding polymethyl-substituted benzene mono-, di-, and triamines with ethyl oxalyl chloride ester in the appropriate 1:1, 1:2, and 1:3 molar ratio, respectively, in the presence of triethylamine [Fig. 5a–c, step (*i*)]. The H_4Et_2L POLs (L = **4a**–**c**) were similarly synthesized from the polymethyl-substituted oxamide-*N,N*′-diphenylamines [Fig. 5d, step (*i*)], which were in turn prepared from the reaction of the corresponding benzene diamines with oxalic acid diethyl ester in a 10:1 molar ratio [Fig. 5d, step (*ii*)].

The hydrogen bond-directed self-assembly of the H_2Et_2**2a** and H_2Et_2**2a**′ POLs, with *meta*- and *para*-substituted phenylene spacers respectively, into either one- (*meso*-helix) or two-dimensional (brick-wall sheet) polymers constitutes a unique example of topological control in self-assembling supramolecular systems in the solid state (Fig. 6a and b) [14,15].

Density functional theory (DFT) calculations on the simpler HMe**1a** POL support the experimental observations on the essential role of hydrogen bonding in determining molecular conforma-

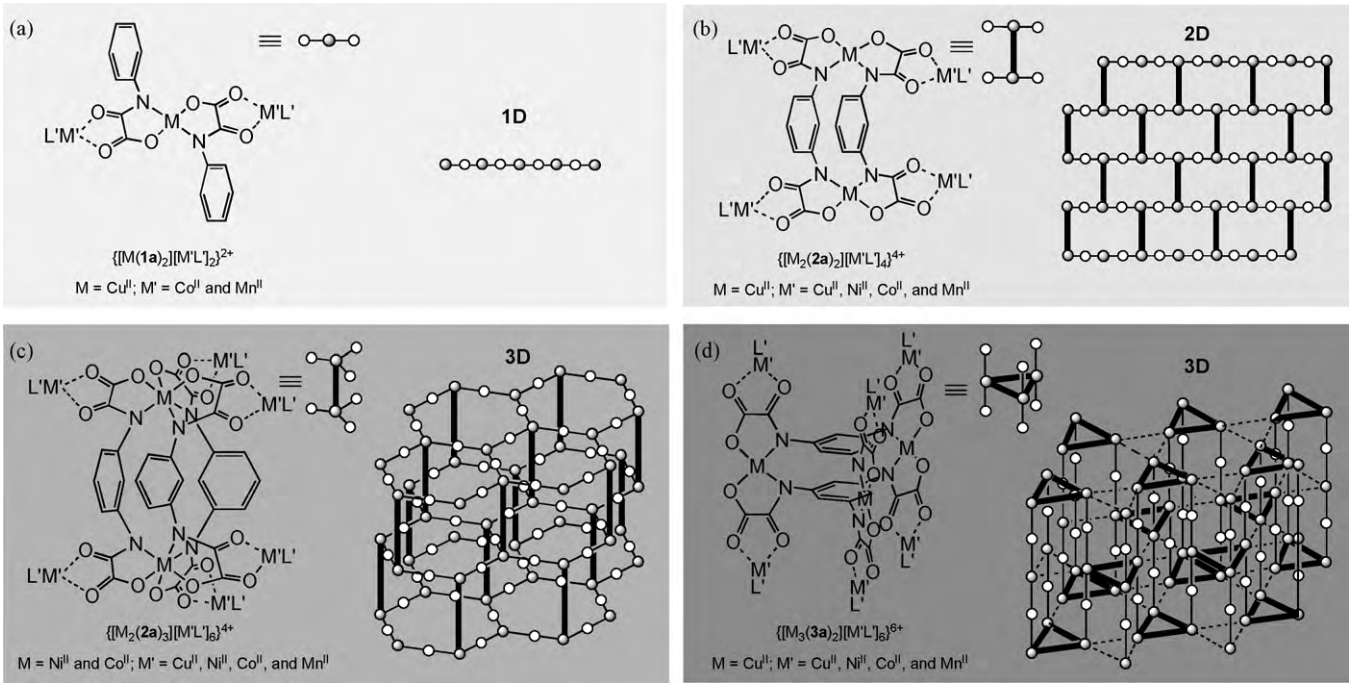

Fig. 4. Self-assembling oxamato-bridged bimetallic MOCs (left) and MOPs (right) with late and middle 3d divalent metal ions: (a) linear trinuclear complexes and 1D ribbon-like chains, (b) ladder-like hexanuclear complexes and 2D brick-wall layers, (c) double-star octanuclear complexes and 3D hexagonal diamond networks, (d) cylinder-like enneanuclear complexes and 3D trigonal networks.

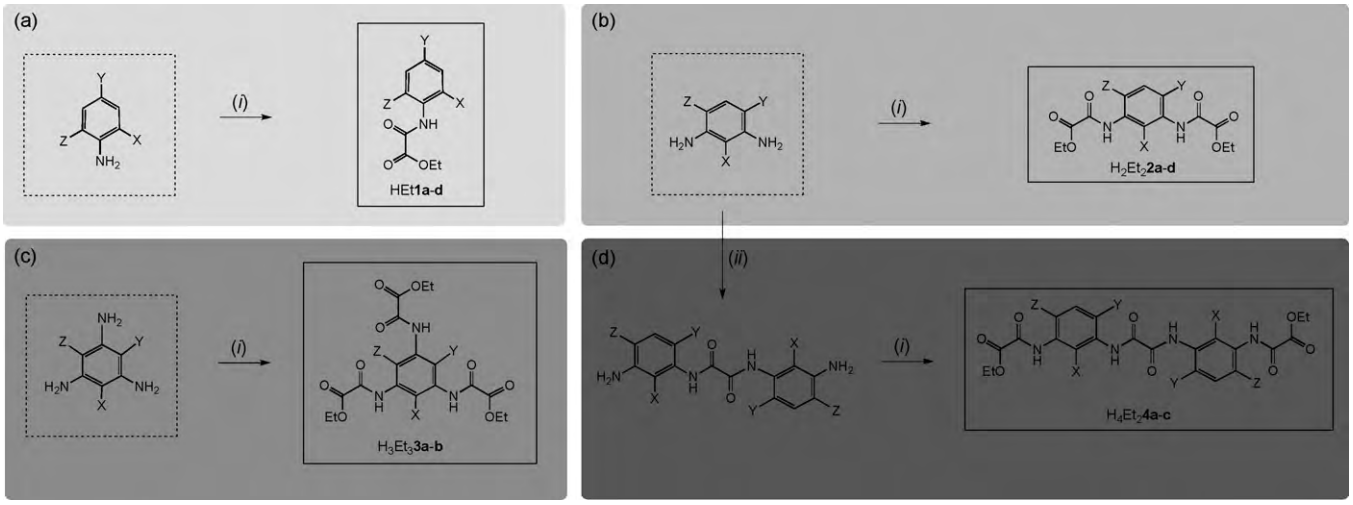

Fig. 5. Synthetic procedure for the preparation of the polyethyl ester acid derivatives of the APOXA ligands from the corresponding aromatic polyamine precursors. Reaction conditions: (*i*) $C_2O_2Cl(OEt)$, Et_3N, THF (80 °C); (*ii*) $C_2O_2(OEt)_2$ (120 °C).

tion and molecular aggregation of the H_2Et_2**2a** and H_2Et_2**2a**′ POLs [15]. Thus, there exists a small but non-negligible electron density delocalization in the central region of the hydrogen-bonded dimer [HMe**1a**]$_2$, which reflects the redistribution of charge that occurs upon hydrogen bond formation in the system (Fig. 6c). This bonding scheme is not consistent with a purely electrostatic formulation, but with a partially covalent nature of the interaction between the hydrogen and the oxygen acceptor atom in the intermolecular N–H···O=C hydrogen bond. We are currently investigating the hydrogen bond-directed self-assembly of the larger, linear H_4Et_2**3a** and triangular H_3Et_3**4a** POLs, with C_3 and C_2 molecular symmetries, respectively, for the elaboration of higher dimensionality ordered structures from molecules (supramolecular solids), which is a main goal in the field of crystal design and crystal engineering [2].

4. Oligonuclear metal–organic ligands (MOLs): from molecular magnetic wires to molecular magnetic switches

Homometallic M^{II}_n MOLs (M = Cu, Ni, and Co; n = 1–3) of varying nuclearity, ranging from mono- to trinuclear, have been rationally prepared from mono-, bis-, and trisbidentate POLs (L = **1b–d**, **2a–d**, **2a**′**–c**′, **3a**, and **4a–c**) and late 3d M^{II} ions, from copper to cobalt, with various preferred coordination geometries (Table 1).

4.1. Double-stranded mononuclear MOLs

Thus, double-stranded Cu^{II} MOLs may be readily obtained from the coordination of the bidentate POLs (L = **1b–d**) to a square-planar Cu^{II} ion in a *trans* disposition (Fig. 7a) [16,17]. Each of the two POLs adopts a non-planar orthogonal conformation with the benzene

Table 1
Selected magnetic data for the MOLs.

Compound	n[a]	J[b] (cm^{-1})	θ[c] (K)	S	D[d] (cm^{-1})
$Na_2[Cu(\mathbf{1b})_2]\cdot 2H_2O$	1		−0.07	1/2	
$(Ph_4P)_2[Cu(\mathbf{1b})_2]\cdot 2H_2O$	1		<0.01	1/2	
$Na_2[Cu(\mathbf{1c})_2]\cdot 2H_2O$	1		−0.08	1/2	
$(Ph_4P)_2[Cu(\mathbf{1c})_2]\cdot 4H_2O$	1		<0.01	1/2	
$Na_2[Cu(\mathbf{1d})_2]\cdot 6H_2O$	1		−0.09	1/2	
$(Ph_4P)_2[Cu(\mathbf{1d})_2]\cdot 4H_2O$	1		<0.01	1/2	
$Na_4[Cu_2(\mathbf{2a})_2]\cdot 10H_2O$	2	+16.8		1	
$(Ph_4P)_4[Cu_2(\mathbf{2a})_2]\cdot 4H_2O$	2	+16.5		1	
$K_4[Cu_2(\mathbf{2b})_2]\cdot 11H_2O$	2	+13.8	−0.59	1	
$(Ph_4P)_4[Cu_2(\mathbf{2b})_2]\cdot 10H_2O$	2	+18.1		1	
$Na_4[Cu_2(\mathbf{2c})_2]\cdot 12H_2O$	2	+9.4		1	
$Li_4[Cu_2(\mathbf{2d})_2]\cdot 14H_2O$	2	+15.6	−0.48	1	
$Na_4[Cu_2(\mathbf{2d})_2]\cdot 9H_2O$	2	+12.8	−0.31	1	
$K_4[Cu_2(\mathbf{2d})_2]\cdot 3H_2O$	2	+14.5		1	
$(Bu_4N)_4[Cu_2(\mathbf{2d})_2]\cdot 12H_2O$	2	+15.9	−0.17	1	
$Li_4[Cu_2(\mathbf{2a}')_2]\cdot 10H_2O$	2	−95		0	
$Na_4[Cu_2(\mathbf{2a}')_2]\cdot 11H_2O$	2	−81		0	
$(Ph_4P)_4[Cu_2(\mathbf{2a}')_2]\cdot 8H_2O$	2	−94		0	
$Li_4[Cu_2(\mathbf{2b}')_2]\cdot 8H_2O$	2	−100		0	
$(Ph_4P)_4[Cu_2(\mathbf{2b}')_2]\cdot 8H_2O$	2	−125		0	
$Li_4[Cu_2(\mathbf{2c}')_2]\cdot 9H_2O$	2	−130		0	
$(Ph_4P)_4[Cu_2(\mathbf{2c}')_2]\cdot 5H_2O$	2	−144		0	
$Li_8[Ni_2(\mathbf{2a})_3]\cdot 37H_2O$	2	+3.2		2	−3.4
$Na_8[Ni_2(\mathbf{2a})_3]\cdot 12H_2O$	2	+3.6		2	−3.5
$Li_8[Ni_2(\mathbf{2c})_3]\cdot 18H_2O$	2	+2.8		2	−4.4
$Na_8[Ni_2(\mathbf{2c})_3]\cdot 12H_2O$	2	+3.8		2	−3.4
$Li_8[Co_2(\mathbf{2a})_3]\cdot 37H_2O$	2	+1.0		3	108
$Na_8[Co_2(\mathbf{2a})_3]\cdot 12H_2O$	2	+1.3		3	109
$Li_6[Cu_3(\mathbf{4a})_2]\cdot 10H_2O$	3	+7.0	−0.90	3/2	
$(Ph_4P)_6[Cu_3(\mathbf{4a})_2]\cdot 6H_2O$	3	+4.9	−0.50	3/2	
$Na_6[Cu_3(\mathbf{4b})_2]\cdot 20H_2O$	3	+12.5	−0.39	3/2	
$(Ph_3EtP)_6[Cu_3(\mathbf{4b})_2]\cdot 14H_2O$	3	+17.1		3/2	
$Na_6[Cu_3(\mathbf{4c})_2]\cdot 25H_2O$	3	+6.9	−0.38	3/2	
$Na_{12}[Co_3(\mathbf{4a})_3]\cdot 33H_2O$	3	+1.2		7/2	120
$Na_{11}[Co_3(\mathbf{4a})_3]\cdot 30H_2O$	3	0		3/2	239
$Li_6[Cu_3(\mathbf{3a})_2]\cdot 8H_2O$	3	+7.3	−0.50	3/2	
$Na_6[Cu_3(\mathbf{3a})_2]\cdot 11.5H_2O$	3	+11.6	+0.41	3/2	
$K_6[Cu_3(\mathbf{3a})_2]\cdot 11H_2O$	3	+16.3	+0.23	3/2	

[a] n is the nuclearity.
[b] J is the intramolecular exchange coupling parameter through the phenylene bridges [$\mathbf{H} = \sum_{i=1-n}(-J\mathbf{S}_{M,i}\mathbf{S}_{M,i+1} + D\mathbf{S}^2_{zM,i})$ (M = Ni) or $\mathbf{H} = \sum_{i=1-n}(-J\mathbf{S}_{M,i}\mathbf{S}_{M,i+1} + D\mathbf{L}^2_{zM,i})$ (M = Co)].
[c] θ is the Weiss constant in the mean field approximation.
[d] D is the local axial magnetic anisotropy parameter [$\mathbf{H} = \sum_{i=1-n}(-J\mathbf{S}_{M,i}\mathbf{S}_{M,i+1} + D\mathbf{S}^2_{zM,i})$ (M = Ni) or $\mathbf{H} = \sum_{i=1-n}(-J\mathbf{S}_{M,i}\mathbf{S}_{M,i+1} + D\mathbf{L}^2_{zM,i})$ (M = Co)].

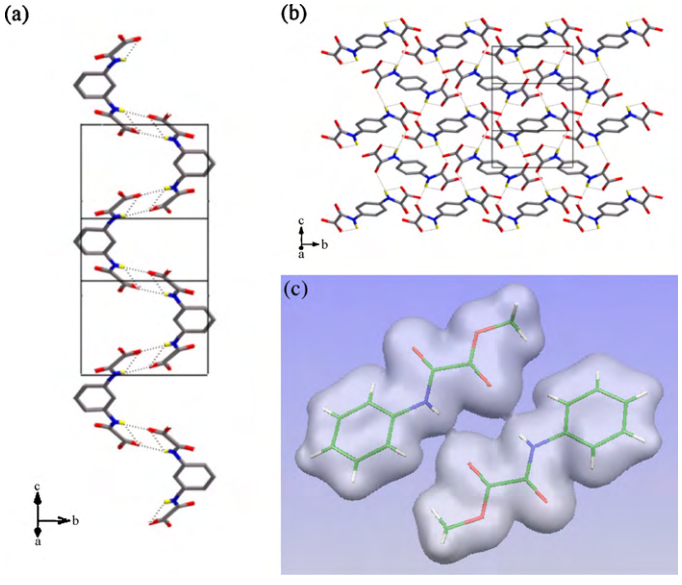

Fig. 6. Structures of a *meso*-helical chain (a) and a brick-wall sheet (b) of hydrogen-bonded neutral ligands of H_2Et_2**2a** and H_2Et_2**2a**′, respectively. Ligand atoms are represented by sticks (C, gray; N, blue; O, red). (c) Electron density distribution for the dimer model of hydrogen-bonded neutral ligands of HMe**1a**.

ring being disposed almost perpendicularly to the oxamato group because of the steric effects of the methyl substituents.

DFT calculations on the simpler Cu^{II} MOL (L = **1a**) show a large spin delocalization of the unpaired electron of the square-planar Cu^{II} ion onto the σ-type orbitals of the oxamato groups. However, a weak but non-negligible spin polarization is present in the π-type orbitals of the orthogonally disposed benzene rings (Fig. 7b). This simple picture announces the distinct σ- and π-orbital pathways governing the mechanism of the exchange interaction through the oxamato and aromatic bridges, respectively, in the resulting MOCs and MOPs as shown below.

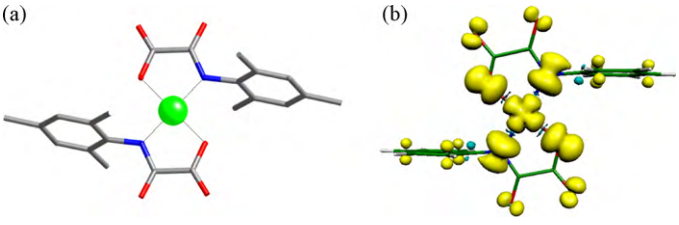

Fig. 7. (a) Structure of the anionic mononuclear unit of $Na_2[Cu(\mathbf{1d})2]\cdot 6H_2O$. Ligand and metal atoms are represented by sticks and balls, respectively (C, gray; N, blue; O, red; Cu, green). (b) Spin density distribution for the ground doublet spin state of $Na_2[Cu(\mathbf{1a})2]\cdot 6H_2O$. Yellow and blue contours represent positive and negative spin densities, respectively.

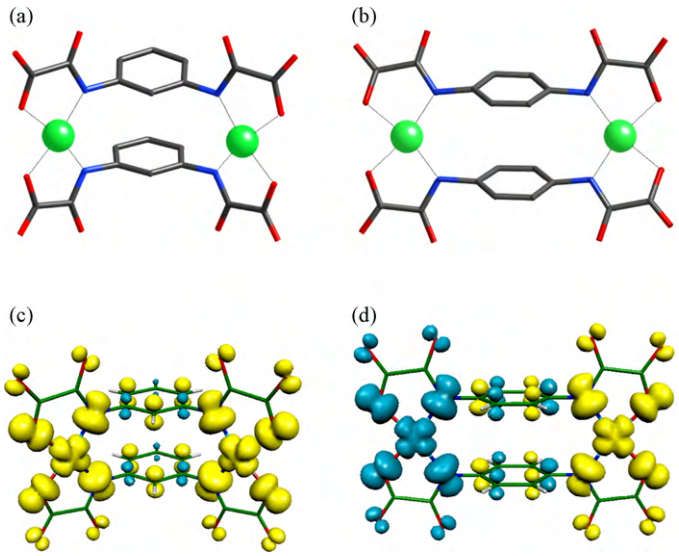

Fig. 8. Structures of the (a) *meta*- and (b) *para*-cyclophane-type anionic dinuclear units of $Na_4[Cu_2(\mathbf{2a})_2]\cdot 10H_2O$ and $Na_4[Cu_2(\mathbf{2a}')_2]\cdot 11H_2O$, respectively. Ligand and metal atoms are represented by sticks and balls, respectively (C, gray; N, blue; O, red; Cu, green). Spin density distributions for the ground (c) triplet and (d) BS singlet spin states of $Na_4[Cu_2(\mathbf{2a})_2]\cdot 10H_2O$ and $Na_4[Cu_2(\mathbf{2a}')_2]\cdot 11H_2O$, respectively. Yellow and blue contours represent positive and negative spin densities, respectively.

4.2. Linear double-stranded di- and trinuclear MOLs

The side-by-side coordination of the C_2-symmetric, bis-bidentate POLs (L = **2a**–**d** and **2a**′–**c**′) to the square-planar Cu^{II} ions leads to double-stranded Cu^{II}_2 MOLs of approximate C_{2v} (L = **2a**–**d**) and D_{2h} (L = **2a**′–**c**′) molecular symmetry (Fig. 8a and b) [18,19]. Interestingly, they possess a metallacyclic structure of *meta*- and *para*-cyclophane-type with a face-to-face *syn* arrangement of the benzene rings from each POL.

These Cu^{II}_2 MOLs show moderate ferro- (L = **2a**–**d**) and strong antiferromagnetic (L = **2a**′–**c**′) couplings between the two Cu^{II} ($S_{Cu} = 1/2$) ions separated by 6.8 and 7.9 Å across the double 1,3- and 1,4-phenylenebis(amidate) bridges, respectively, leading to $S = 1$ and $S = 0$ ground spin states (Table 1) [18,19]. Both effects result from the spin density alternation in the π-conjugated bond system of the phenylene spacers with *meta*- and *para*-substitution patterns (spin polarization mechanism) (Fig. 8c and d). These dicopper(II) metallacyclophanes thus constitute unique examples of the spin control in metal complexes by the topology of the bridging ligand [20].

Similarly, the side-by-side coordination of the larger C_2-symmetric, tris-bidentate POLs (L = **4a**–**c**) to the square-planar Cu^{II} ions leads to the related double-stranded Cu^{II}_3 MOLs of approximate D_2 molecular symmetry (Fig. 9a) [21]. In this case, however, the two adjacent metallacyclophane cores of *meta*-cyclophane-type possess a face-to-face *anti* arrangement of the benzene rings from each POL. These Cu^{II}_3 MOLs show a $S = 3/2$ ground spin state as a result of the ferromagnetic coupling between the three linearly disposed Cu^{II} ($S_{Cu} = 1/2$) ions separated by 7.3 Å, in agreement with a spin polarization mechanism across the double 1,3-phenylenebis(amidate) bridge within each of the two metallacyclophane cores (Table 1) [21].

This series of linear double-stranded Cu^{II}_n MOLs (L = **2a**–**d** and **4a**–**c**) with $S = 1/2 \times n$ ground states ($n = 2$ and 3) constitutes the metal–organic analogues of purely organic, linear high-spin polyradicals (so-called "polaronic ferromagnets") [22]. In this case, the square-planar copper(II)-bis(oxalamide) moieties serve as spin-containing units while the two *meta*-substituted phenylene spacers act as ferromagnetic coupling unit (FCU) (Fig. 9b). They

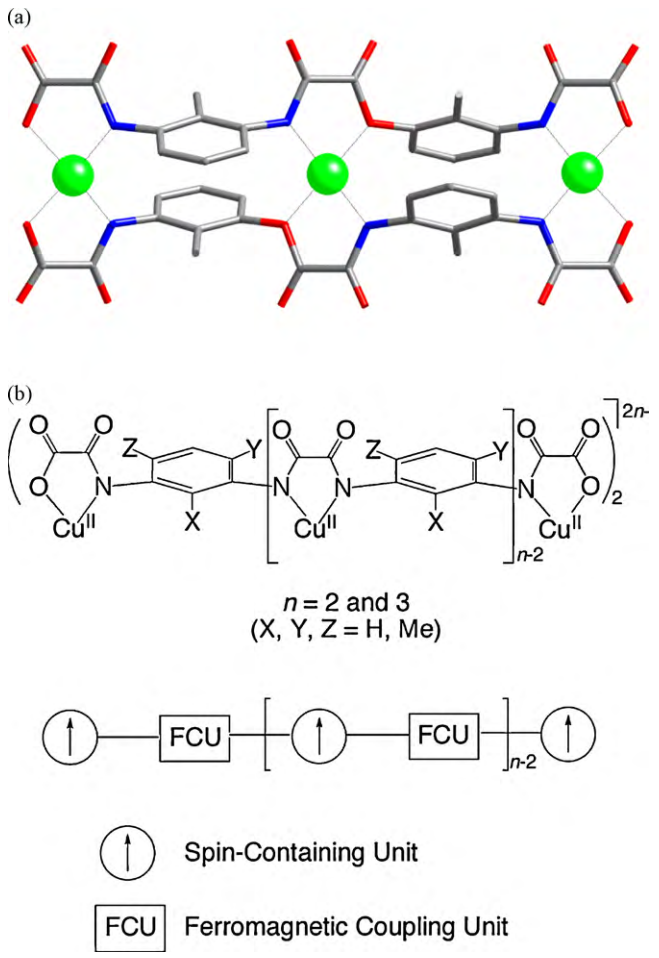

Fig. 9. (a) Structure of the anionic trinuclear unit of $(Ph_3EtP)_6[Cu_3(\mathbf{4b})_2]\cdot 14H_2O$ with two adjacent metallacyclophane cores. Ligand and metal atoms are represented by sticks and balls, respectively (C, gray; N, blue; O, red; Cu, green). (b) Spin coupling model for the Cu^{II}_n MOLs ($n = 2$ and 3).

behave thus as effective "metal–organic wires" (MOWs), whereby a ferromagnetic interaction is propagated along the linear chain of metal ions with intermetallic distances in the range 0.7–1.5 nm [21].

4.3. Linear triple-stranded di- and trinuclear MOLs

Alternatively, the side-by-side coordination of the C_2-symmetric, bis-bidentate POLs (L = **2a** and **2c**) to octahedral M^{II} ions (M = Ni and Co) leads to triple-stranded M^{II}_2 MOLs with a unique metallacyclic structure of metallacryptand-type having an edge-to-face arrangement of the benzene rings (Fig. 10a) [23]. In this case, the unique formation of dinuclear metallacryptands with a *meso*-helicate-like architecture (so-called mesocates) of C_{3h} molecular symmetry leads to alternating (Λ,Δ) chiralities for the octahedral M^{II} ions. This situation is favored because the relatively short and rigid character of the phenylene spacer prevents helical twisting of each POL around the octahedral metal centers with identical (Λ,Λ) or (Δ,Δ) chiralities to give the more common helicates of D_{3d} molecular symmetry [3c].

These M^{II}_2 MOLs (L = **2a** and **2c**) possess $S = 2$ (M = Ni) or $S = 3$ (M = Co) ground spin states as a result of the moderate to weak ferromagnetic coupling between the two high-spin Ni^{II} ($S_{Ni} = 1$) or Co^{II} ($S_{Co} = 3/2$) ions separated by 6.8 and 6.9 Å, respectively, through the triple *meta*-substituted phenylenediamidate bridge (Table 1) [23]. At this respect, the successful extension to these dinickel(II)

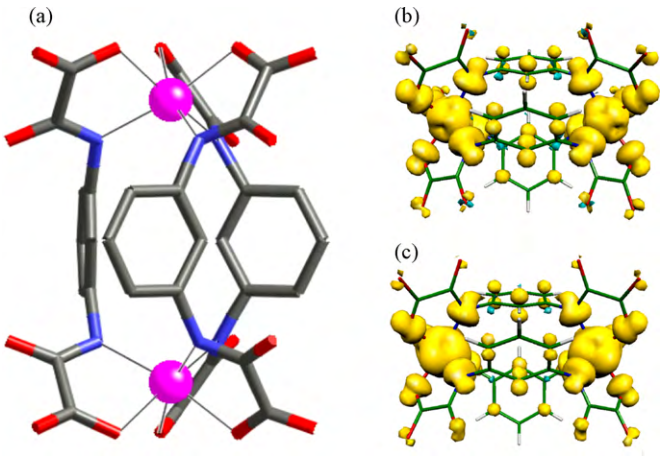

Fig. 10. (a) Structure of the *meso*-helicate-type anionic dinuclear unit of $Na_8[M_2(\mathbf{2a})_3]\cdot 12H_2O$ (M = Ni and Co) with a metallacryptand core. Ligand and metal atoms are represented by sticks and balls, respectively (C, gray; N, blue; O, red; M, purple). Spin density distributions for the ground (b) quintet and (c) septet spin states of $Na_8[Ni_2(\mathbf{2a})_3]\cdot 12H_2O$ and $Na_8[Co_2(\mathbf{2a})_3]\cdot 12H_2O$, respectively. Yellow and blue contours represent positive and negative spin densities, respectively.

and dicobalt(II) metallacryptands of the spin polarization approach to ferromagnetism supports the general validity of this strategy for late 3d metal ions (Fig. 10b and c). This approach to ferromagnetism based on the interaction between spin densities of different signs issued from spin polarization effects by the metal ions across the organic spacers is particularly appealing; however, it has received limited attention in the context of polynuclear metal complexes [24].

Similarly, the side-by-side coordination of the larger C_2-symmetric, tris-bidentate POL (L = **4a**) to the octahedral Co^{II} ions leads to the related triple-stranded $Co^{II}{}_3$ MOL of approximate D_3 molecular symmetry (Fig. 11a) [25]. As for the parent triple-stranded $Co^{II}{}_2$ MOL (L = **2a**), it possesses a *meso*-helicate structure with a racemic mixture of heterochiral triple mesocates of alternating (Λ,Δ,Λ) and (Δ,Λ,Δ) chiralities for the linearly disposed octahedral Co^{II} ions being present in the solid state. This situation contrasts with the more common examples of homochiral (Λ,Λ,Λ) or (Δ,Δ,Δ) triple helicates, which would result instead from helical wrapping of the POLs around the octahedral metal centers [3c].

This $Co^{II}{}_3$ MOL (L = **4a**) presents two redox states with dramatically different magnetic properties (Fig. 11b) [25]. Hence, a weak but non-negligible ferromagnetic coupling exists between the central low-spin Co^{II} ion ($S_{Co} = 1/2$) and the terminal high-spin Co^{II} ions ($S_{Co} = 3/2$) separated by an intermetallic distance of 6.9 Å, in agreement with a spin polarization mechanism across the triple *meta*-substituted phenylenebis(amidate) bridge within each of the two metallacryptand cores (Table 1). On the contrary, there is no sign of either ferro- or antiferromagnetic coupling between the two terminal high-spin Co^{II} ions ($S_{Co} = 3/2$) upon one-electron oxidation of the central low-spin Co^{II} ion ($S_{Co} = 1/2$) to a diamagnetic low-spin Co^{III} ion ($S_{Co} = 0$), as expected given the large intermetallic distance of 13.8 Å (Table 1). This unique redox couple of linear triple-stranded $Co^{II}{}_3$ and $Co^{II}{}_2Co^{III}$ MOLs behave thus as effective electrically triggered "metal–organic switches" (MOSs). In fact, the spins of the metal centers are ferromagnetically coupled in the homovalent tricobalt(II) triple mesocate ("ON" state), whereas they are uncoupled in the heterovalent tricobalt(II,III,II) triple mesocate ("OFF" state) [25].

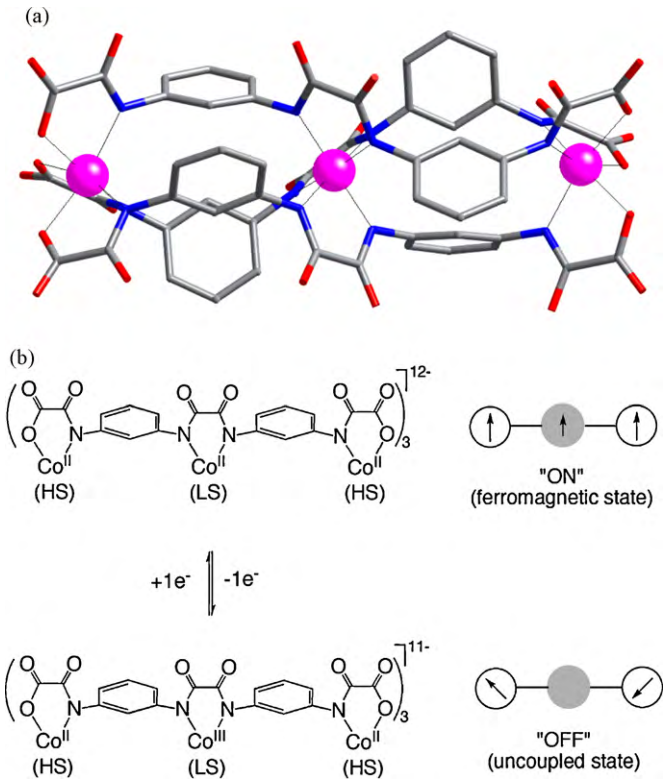

Fig. 11. (a) Structure of the *meso*-helicate-type anionic trinuclear unit of $Na_{12}[Co_3(\mathbf{4a})_3]\cdot 33H_2O$ with two adjacent metallacryptand cores. Ligand and metal atoms are represented by sticks and balls, respectively (C, gray; N, blue; O, red; Co, purple). (b) Spin coupling model for the $Co^{II}{}_3$ and $Co^{II}{}_2Co^{III}$ MOLs.

4.4. Triangular cage-like trinuclear MOLs

When the related C_3-symmetric, tris-bidentate POL (L = **3a**) coordinate to square-planar Cu^{II} ions, a $Cu^{II}{}_3$ MOL with a unique triangular cage-like metallacyclic structure of [3.3.3](1,3,5)cyclophane-type and pseudo-D_{3h} molecular symmetry is obtained (Fig. 12a) [26]. This $Cu^{II}{}_3$ MOL, which contains three triangularly disposed Cu^{II} ($S_{Cu} = 1/2$) ions separated by 6.9–7.1 Å, exhibits a $S = 3/2$ ground spin state as a result of spin polarization effects across the double 1,3,5-benzenetriyl-tris(amidate) bridge (Fig. 12b) [26].

This family of self-assembled $M^{II}{}_n$ MOLs (M = Cu, Ni, and Co; L = **2a–d**, **2a′–c′**, **3a**, and **4a–c**; $n = 2$ and 3) provides thus one of the rare systematic studies on the magnetochemistry of exchange-coupled metallacyclic complexes with late 3d M^{II} ions (Table 1). Overall, we have shown that aromatic spacers are really effective

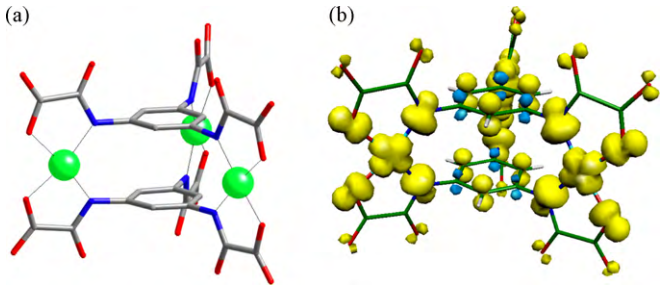

Fig. 12. (a) Structure of the anionic trinuclear unit of $K_6[Cu_2(\mathbf{3a})_2]\cdot 11H_2O$ with a triangular cage-type metallacyclophane core. Ligand and metal atoms are represented by sticks and balls, respectively (C, gray; N, blue; O, red; Cu, green). (b) Spin density distribution for the ground quartet spin state of $K_6[Cu_2(\mathbf{3a})_2]\cdot 11H_2O$. Yellow and blue contours represent positive and negative spin densities, respectively.

to mediate magnetic exchange interactions between paramagnetic metal centers separated by relatively long intermetallic distances in a discrete metallacyclic entity [18,19]. Furthermore, we have demonstrated that the appropriate choice of the electronic configuration of the metal ion and the topology of the bridging ligand allows us to control the nature and magnitude of the magnetic coupling between the metal centers through the aromatic spacer in the corresponding di- and trinuclear metallacycles [18,19,23,26].

Besides their interest as models for the fundamental research on electron exchange phenomena between distant metal centers through extended bridges, some of these oligonuclear MOLs would be also relevant as molecular spintronic devices. At this regard, the linear M^{II}_3 MOLs (M = Cu and Co; L = **4a**–**c**) are potential candidates to molecular magnetic wires (MMWs) and molecular magnetic switches (MMSs) for the transmission of through-bond metal–metal electron exchange interactions [21,25], by analogy with related molecular wires and switches based on direct metal–metal electron transfer interactions instead [27]. In contrast to conventional molecular electronic devices, these MMWs and MMSs may offer a new design concept for the transport and processing of information over long distances based on purely electron exchange (Coulomb) interactions and involving no current flow.

5. High-nuclearity metal–organic clusters (MOCs): from high-spin molecules to single-molecule magnets

Homo- and heterobimetallic $M^{II}_n M'^{II}_m$ MOCs (M and M′ = Cu, Ni, and Co; n = 2 and 3; m = 3, 4, and 6) of varying nuclearity, ranging from penta- to enneanuclear species, have been rationally prepared starting from M^{II}_2 (M = Cu, Ni, and Co; L = **2a**–**d** and **2a**′) and Cu^{II}_3 (L = **3a**) MOLs. In these cases, they act as tris-, tetrakis-, or hexakis-bidentate MOLs toward coordinatively unsaturated M'^{II} complexes (M′ = Cu and Ni) with different acyclic (L′ = Me_4en, Me_5dien, dipn, and trien) and macrocyclic (L′ = Me_3tacden and cyclam) aliphatic polyamines as blocking ligands (Table 2).

5.1. Penta- and hexanuclear ladder-like MOCs

The Cu^{II}_6 MOCs (L = **2a**, **2d**, and **2a**′; L′ = Me_4en and Me_5dien) exhibit a "dimer-of-trimers" ladder-like structure of approximate C_{2v} (L = **2a** and **2d**) or D_{2h} (L = **2a**′) molecular symmetry (Fig. 13a and b) [28,29]. In this case, the nature of the ground spin state can be rationally interpreted based on the concept of antiferro- (ACU) and ferromagnetic coupling units (FCU) which was earlier used to control the spin in organic polyradicals [30]. Thus, the Cu^{II}_2 *meta*- and *para*-cyclophane cores act as FCU and ACU, respectively, between the two Cu^{II}_3 linear entities ($S_A = S_B = 2S_{Cu} - S_{Cu} = 1/2$) leading to either a ground triplet ($S = S_A + S_B = 1$) or a singlet ($S = S_A - S_B = 0$) spin state for the Cu^{II}_6 molecule (Fig. 13c–e) [28,29].

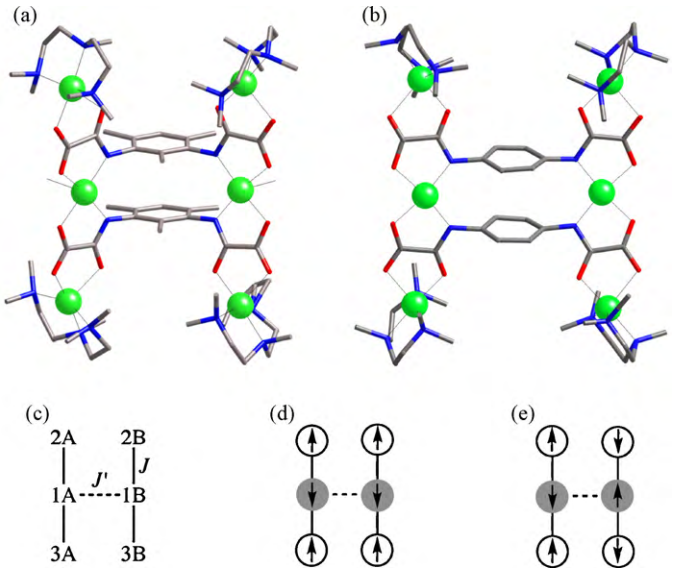

Fig. 13. Structures of the ladder-like cationic hexanuclear unit of (a) $\{[Cu_2(\mathbf{2d})_2(H_2O)_2][Cu(Me_5dien)]_4\}(ClO_4)_4\cdot 12H_2O$ and (b) $\{[Cu_2(\mathbf{2a}')_2][Cu(Me_5dien)]_4\}(ClO_4)_4$ with dinuclear *meta*- and *para*-cyclophane cores, respectively. Ligand and metal atoms are represented by sticks and balls, respectively (C, gray; N, blue; O, red; Cu, green). (c) Spin coupling scheme and spin topologies for the Cu^{II}_6 MOCs with $J < 0$ and either (d) $J' > 0$ or (e) $J' < 0$.

In the $Cu^{II}_2Ni^{II}_3$ MOCs (L = **2a**; L′ = Me_3tacden and cyclam) with an incomplete "dimer-plus-trimer" ladder-like structure of reduced C_1 molecular symmetry (Fig. 14a), the Cu^{II}_2 metacyclophane core also acts as a FCU between the $Cu^{II}Ni^{II}$ ($S_A = S_{Ni} - S_{Cu} = 1/2$) and $Cu^{II}Ni^{II}_2$ ($S_B = 2S_{Ni} - S_{Cu} = 3/2$) linear entities affording a ground quintet spin state ($S = S_A + S_B = 2$) for the $Cu^{II}_2Ni^{II}_3$ molecule (Table 2) [29].

5.2. Octanuclear double-star MOCs

The $M^{II}_2Cu^{II}_6$ MOCs (M = Cu, Ni, and Co; L = **2a** and **2c**; L′ = Me_5dien) have a "dimer-of-tetramers" double-star structure of approximate C_{3h} molecular symmetry (Fig. 15a) [31,32]. In this case, the M^{II}_2 metallacryptand cores act as ACUs between the two $M^{II}Cu^{II}_3$ star entities [$S_A = S_B = 3S_{Cu} - S_M = 1$ (M = Cu), 1/2 (M = Ni), and 0 (M = Co)] leading to a ground singlet spin state ($S = S_A - S_B = 0$) for the $M^{II}_2Cu^{II}_6$ molecule (Fig. 15b and c) [31,32].

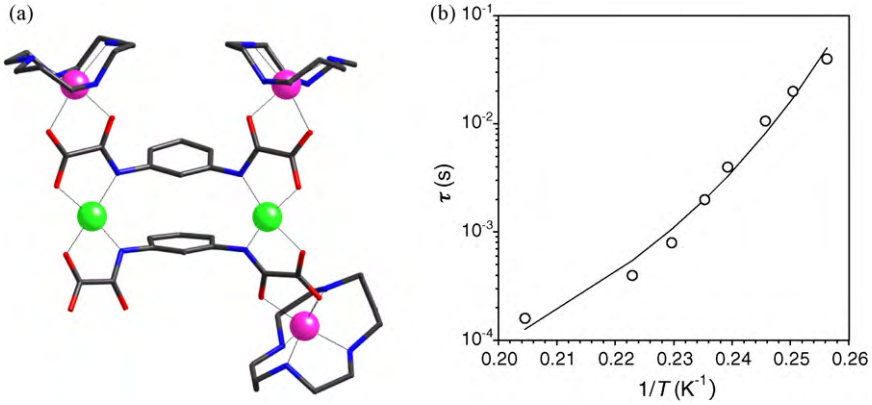

Fig. 14. (a) Structure of the incomplete ladder-like cationic pentanuclear unit of $[Ni(cyclam)]\{[Cu_2(\mathbf{2a})_2][Ni(cyclam)]_3\}(ClO_4)_4\cdot 6H_2O$ with a dinuclear metallacyclophane core. Ligand and metal atoms are represented by sticks and balls, respectively (C, gray; N, blue; O, red; Cu, green; Ni, purple). (b) Arrhenius plot for $\{[Cu_2(\mathbf{2a})_2][Ni(Me_3tacden)]_3\}(ClO_4)_2\cdot 10H_2O$. The solid line is the best-fit curve (see Table 2).

Table 2
Selected magnetic data for the MOCs.

Compound[a]	n[b]	J[c] (cm^{-1})	J'[c] (cm^{-1})	θ[d] (K)	S	D[e] (cm^{-1})	T_B[f] (K)	E_a[g] (cm^{-1})	τ_0[h] (s)	T_0[i] (K)	F[j]
$\{[Cu_2(\mathbf{2a})_2][Cu(Me_4en)]_4\}(ClO_4)_4\cdot 6H_2O$	6	−288.3	+15.5		1						
$\{[Cu_2(\mathbf{2a})_2(H_2O)F][Cu(Me_5dien)]_4\}(PF_6)_3\cdot 4H_2O$	6	−105.9	+1.7		1						
$\{[Cu_2(\mathbf{2d})_2(H_2O)_2][Cu(Me_5dien)]_4\}(ClO_4)_4\cdot 12H_2O$	6	−92.6	+9.0		1						
$\{[Cu_2(\mathbf{2a}')_2][Cu(Me_5dien)]_4\}(ClO_4)_4$	6	−81.3	−120.6		0						
$\{[Cu_2(\mathbf{2a})_2][Ni(Me_3tacden)]_3\}(ClO_4)_2\cdot 10H_2O$	5	−158.0	+15.0	+1.5	2		5.0	6.8 (79.9)	0.7×10^{-6} (0.6×10^{-14})	3.0	0.08
$[Ni(cyclam)]\{[Cu_2(\mathbf{2a})_2][Ni(cyclam)]_3\}(ClO_4)_4\cdot 6H_2O$	5	−111.6	+4.2		2						
$Na_2\{[Cu_2(\mathbf{2a})_3][Cu(Me_5dien)]_6\}(ClO_4)_6\cdot 12H_2O$	8	−57.0	−28.0		0						
$Na_2\{[Cu_2(\mathbf{2c})_3][Cu(Me_5dien)]_6\}(ClO_4)_6\cdot 12H_2O$	8	−52.0	−48.0		0						
$Na_2\{[Ni_2(\mathbf{2a})_3][Cu(Me_5dien)]_6\}(ClO_4)_6\cdot 17H_2O$	8	−39.1	−0.2		0						
$Na_2\{[Ni_2(\mathbf{2c})_3][Cu(Me_5dien)]_6\}(ClO_4)_6\cdot 17H_2O$	8	−44.7	−0.4		0						
$Na_2\{[Co_2(\mathbf{2a})_3][Cu(Me_5dien)]_6\}(ClO_4)_6\cdot 22H_2O$	8	−17.0	−1.0		0						
$\{[Ni_2(\mathbf{2a})_3][Ni(dipn)(H_2O)]_6\}(ClO_4)_4\cdot 12.5H_2O$	8	−26.6	+3.1		4	−0.23	4.5	4.0 (101.6)	1.4×10^{-6} (1.3×10^{-16})	2.5	0.05
$\{[Ni_2(\mathbf{2c})_3][Ni(dipn)(H_2O)]_6\}(ClO_4)_4\cdot 12.5H_2O$	8	−26.3	+2.1		4						
$\{[Ni_2(\mathbf{2a})_3][Ni(Me_3tacden)]_6\}(ClO_4)_4\cdot 10H_2O$	8	−22.1	−3.3		0						
$\{[Ni_2(\mathbf{2a})_3][Ni(cyclam)]_6\}(ClO_4)_4\cdot 6H_2O$	8	−22.2	+16.7		4						
$\{[Cu_3(\mathbf{3a})_2][Cu(Me_4en)]_6\}(ClO_4)_6\cdot 9H_2O$	9	−318.0	+7.9	+1.2	3/2						
$\{[Cu_3(\mathbf{3a})_2][Cu(Me_5dien)]_6\}(ClO_4)_6\cdot 12H_2O$	9	−106.0	+7.8		3/2						
$\{[NiCu_2(\mathbf{3a})_2][Cu(Me_5dien)]_6\}(ClO_4)_6\cdot 13H_2O$	9	−81.3 (−39.7)	+20.7	−0.3	1						
$\{[Ni_2Cu(\mathbf{3a})_2][Cu(Me_5dien)]_6\}(ClO_4)_6\cdot 14H_2O$	9	−110.2 (−44.3)		−0.2	1/2						
$\{[Cu_3(\mathbf{3a})_2][Ni(trien)]_6\}(ClO_4)_6\cdot 18H_2O$	9	−37.6	+7.5		9/2		<2.0				

[a] Ligand abbreviations: Me_4en = *N,N,N′,N′*-tetramethylethylenediamine; Me_5dien = *N,N,N′,N″,N″*-pentamethyldiethylenetriamine; dipn = dipropylenetriamine; trien = triethylenetetraamine; $Me_3tacden$ = 2,4,4-trimethyl-1,5,9-triazacyclododec-1-ene; cyclam = 1,4,8,11-tetraazacyclotetradecane.

[b] n is the nuclearity.

[c] J and J' are the exchange coupling parameters through the oxamato and phenylene bridges, respectively [$\mathbf{H} = -\sum_{i=1-n}\sum_{j=1-m}J(\mathbf{S}_{M,i}\mathbf{S}_{M',j}) - \sum_{i=1-n}J'(\mathbf{S}_{M,i}\mathbf{S}_{M,i+1}) + D\mathbf{S}_z^2$]. The J values between distinct metal centers (M = Ni and M′ = Cu) are given in parentheses.

[d] θ is the Weiss constant in the mean field approximation.

[e] D is the global axial magnetic anisotropy parameter [$\mathbf{H} = -\sum_{i=1-n}\sum_{j=1-m}J(\mathbf{S}_{M,i}\mathbf{S}_{M',j}) - \sum_{i=1-n}J'(\mathbf{S}_{M,i}\mathbf{S}_{M,i+1}) + D\mathbf{S}_z^2$].

[f] T_B is the blocking temperature calculated as the temperature of the maximum of χ''_M at ν = 1000 Hz ($T_B = T_{max}$).

[g] E_a is the activation energy for the magnetization reversal calculated through the Vogel–Fulcher law ($\tau = \tau_0\exp[E_a/k_B(T-T_0)]$). The E_a values calculated from the Arrhenius law ($T_0 = 0$) are given in parentheses.

[h] τ_0 is the preexponential factor calculated through the Vogel–Fulcher law ($\tau = \tau_0\ \exp[E_a/k_B(T-T_0)]$). The τ_0 values calculated from the Arrhenius law ($T_0 = 0$) are given in parentheses.

[i] T_0 is the critical temperature in the Vogel–Fulcher law ($\tau = \tau_0\ \exp[E_a/k_B(T-T_0)]$).

[j] F is the Mydosh parameter [$F = (\Delta T_{max}/T_{max})/\Delta(\log\nu)$].

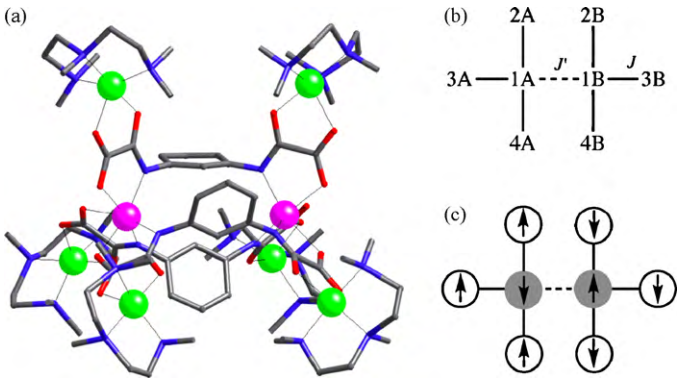

Fig. 15. (a) Structure of the double-star cationic octanuclear unit of $Na_2\{[M_2(\mathbf{2a})_3][Cu(Me_5dien)]_6\}(ClO_4)_6{\cdot}12H_2O$ (M = Cu, Ni, and Co) with a *meso*-helicate-type dinuclear metallacryptand core. Ligand and metal atoms are represented by sticks and balls, respectively (C, gray; N, blue; O, red; Cu, green; M, purple). (b) Spin coupling scheme and (c) spin topology for the $M^{II}{}_2Cu^{II}{}_6$ MOCs (M = Cu, Ni, and Co) with $J<0$ and $J'<0$.

This situation contrasts to that found in the $Ni^{II}{}_8$ MOCs (L = **2a** and **2c**; L′ = dipn) which possesses a "dimer-of-tetramers" double-star structure of reduced C_1 molecular symmetry due to the presence among the six peripheral metal atoms of both *mer* and *fac* isomers with respect to the conformation of the tridentate blocking ligand dipn (Fig. 16a) [33]. In this other case, the $Ni^{II}{}_2$ metallacryptand core acts as a FCU between the $Ni^{II}{}_4$ star entities ($S_A = S_B = 3S_{Ni} - S_{Ni} = 2$) to give a ground nonet spin state ($S = S_A + S_B = 4$) for the $Ni^{II}{}_8$ molecule (Table 2) [33].

5.3. Enneanuclear cylinder-like MOCs

The $Cu^{II}{}_9$ MOCs (L = **3a**; L′ = Me_4en and Me_5dien) have a "trimer-of-trimers" cylinder-like structure of approximate D_3 molecular symmetry (Fig. 17a) [34]. In this case, the triangular $Cu^{II}{}_3$ metallacyclophane core acts as a FCU between the three $Cu^{II}{}_3$ linear entities ($S_A = S_B = S_C = 2S_{Cu} - S_{Cu} = 1/2$) leading to a ground quartet spin state ($S = S_A + S_B + S_C = 3/2$) for the $Cu^{II}{}_9$ molecule (Fig. 17c and d) [34]. Interestingly, the partial substitution of Cu^{II} ($S_{Cu} = 1/2$) by high-spin Ni^{II} ($S_{Ni} = 1$) ions at the triangular metallacyclophane core leads to the $Ni^{II}Cu^{II}{}_8$ and $Ni_2{}^{II}Cu^{II}{}_7$ MOCs (L = **3a**; L′ = Me_5dien) with reduced C_2 molecular symmetries (Fig. 17b) [35]. They possess either a ground triplet ($S = S_A + S_B + S_C = 1$ with $S_A = S_B = 2S_{Cu} - S_{Cu} = 1/2$ and $S_C = 2S_{Cu} - S_{Ni} = 0$) or a doublet ($S = S_A + S_B + S_C = 1/2$ with $S_A = 2S_{Cu} - S_{Cu} = 1/2$ and $S_B = S_C = 2S_{Cu} - S_{Ni} = 0$) spin state for the $Ni^{II}Cu^{II}{}_8$ and $Ni_2{}^{II}Cu^{II}{}_7$ molecules, respectively (Table 2) [35].

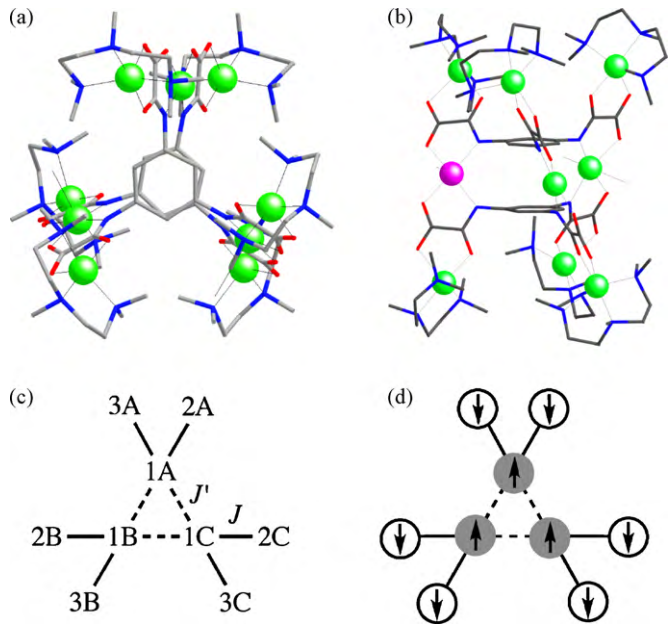

Fig. 17. Structures of the cylinder-like cationic enneanuclear unit of (a) $\{[Cu_3(\mathbf{3a})_2(H_2O)_2][Cu(Me_5dien)]_6\}(ClO_4)_6{\cdot}9H_2O$ and (b) $\{[NiCu_2(\mathbf{3a})_2(H_2O)_4][Cu(Me_5dien)]_6\}(ClO_4)_6{\cdot}9H_2O$ with a triangular cage-type trinuclear metallacyclophane core. Ligand and metal atoms are represented by sticks and balls, respectively (C, gray; N, blue; O, red; Cu, green; Ni, purple). (c) Spin coupling scheme and (d) spin topology for the $Ni^{II}{}_nCu^{II}{}_{(9-n)}$ MOCs (n = 0–2) with $J<0$ and $J'>0$.

Finally, we have prepared the $Cu^{II}{}_3Ni^{II}{}_6$ MOC (L = **3a**; L′ = trien) by replacing the terminal Cu^{II} ($S_{Cu} = 1/2$) by high-spin Ni^{II} ($S_{Ni} = 1$) ions. In this case, the triangular $Cu^{II}{}_3$ metallacyclophane core also acts as a FCU between the three $Cu^{II}Ni^{II}{}_2$ linear entities ($S_A = S_B = S_C = 2S_{Ni} - S_{Cu} = 3/2$) leading to a ground decet spin state ($S = S_A + S_B + S_C = 9/2$) for the $Cu^{II}{}_3Ni^{II}{}_6$ molecule (Table 2).

Besides their fascinating structures and relevant insights into metal-directed self-assembly processes, this family of oxamate-bridged, homo- and heterobimetallic $M^{II}{}_nM'^{II}{}_m$ MOCs (M and M′ = Cu, Ni, and Co; n = 2 and 3; m = 3, 4, and 6) display unique magnetic properties which result from the particular assembling topology of the paramagnetic metal ions by the bridging and terminal ligands. Hence, they have different values of the ground spin state (S = 0–9/2) and the magnetic anisotropy (D) depending on the combination of M^{II} and M'^{II} ions, the substitution pattern of the bridging ligand, either *meta* (L = **2a**–**d** and **3a**) or *para* (L = **2a**′), and the denticity of the blocking ligand, either bi- (L′ = Me_4en), tri-

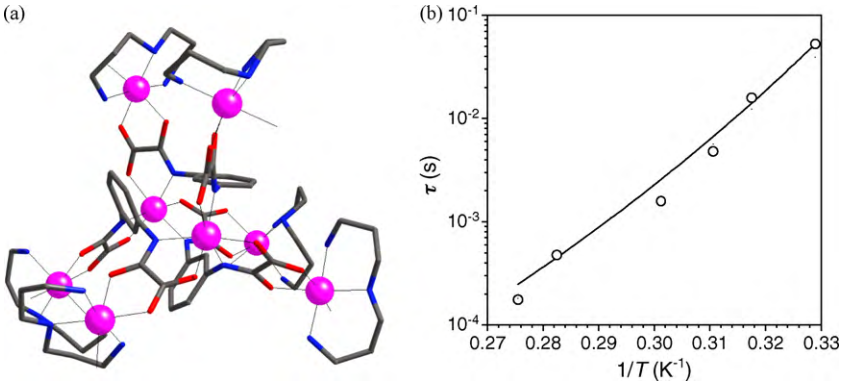

Fig. 16. (a) Structure of the double-star cationic octanuclear unit of $\{[Ni_2(\mathbf{2a})_3][Ni(dipn)(H_2O)]_6\}(ClO_4)_4{\cdot}12.5H_2O$ with a *meso*-helicate-type dinuclear metallacryptand core. Ligand and metal atoms are represented by sticks and balls, respectively (C, gray; N, blue; O, red; Ni, purple). (b) Arrhenius plot for $\{[Ni_2(\mathbf{2a})_3][Ni(dipn)(H_2O)]_6\}(ClO_4)_4{\cdot}12.5H_2O$. The solid line is the best-fit curve (see Table 2).

(L′ = Me_5dien, dipn, and Me_3tacden) or tetradentate (L′ = trien and cyclam) (Table 2). As a matter of fact, nanosized MOCs with either low- ($S = 1/2$) or high-spin ($S \gg 1/2$) ground states are being extensively studied in recent years as unique examples of molecular magnets for future applications in classical or quantum information processing [36,37].

So, the series of $Ni^{II}_nCu^{II}_{(9-n)}$ MOCs (L = **3a**; L′ = Me_5dien) with low-spin $S = (3-n) \times 1/2$ ground states ($n = 0$–2) are potential candidates to multiple quantum bits (Qubits) in information storage and processing [36]. On the other hand, the $Cu^{II}_2Ni^{II}_3$ (L = **2a**; L′ = Me_3tacden) and Ni^{II}_8 (L = **2a**; L′ = dipn) MOCs have moderately anisotropic $S = 2$ and $S = 4$ ground states, respectively, which result from the moderate local magnetic anisotropy of the octahedral high-spin Ni^{II} ions (^3E) and the overall structural anisotropy of these penta- and octanuclear molecules with reduced C_1 symmetry. Interestingly, they exhibit slow magnetic relaxation effects at low temperatures ($T_B < 5.0$ K) that are reminiscent of the so-called single-molecule magnets (SMMs) (Figs. 14b and 16b). This unique SMM behavior, which has no analogy in the world of classical magnets, is not due to a long-range 3D magnetic order but has a pure dynamic origin that is associated with the large axial negative magnetic anisotropy ($D < 0$) of the high-spin molecule [37]. Yet, the relaxation dynamics in the $Cu^{II}_2Ni^{II}_3$ and Ni^{II}_8 MOCs does not follow the Arrhenius law that is typical of genuine SMMs; they present instead a Vogel–Fulcher law dependence that is characteristic of cluster glasses due to the presence of weak intermolecular interactions ($T_0 = 2.5$–3.0 K) in the solid state (Table 2) [38].

We are currently investigating the morphosynthesis of novel hybrid materials from the multilevel organization of these molecules with interesting magnetic properties into suitable ordered host systems (molecular addressing), which is a major current challenge in materials science and nanotechnology [39]. At this respect, silica-based mesoporous materials as well as clay minerals have recently been employed as support hosts for the Ni^{II}_8 MOC [40,41]. While the incorporation of isolated Ni^{II}_8 molecules into single clay platelets took place with the loss of the SMM behavior [41], their incorporation and further aggregation into ordered mesoporous silica led to oligomeric $[Ni^{II}_8]_n$ aggregates of greater spin values ($S = 4n$) and blocking temperatures ($T_B = 4.5$–10.5 K) than those of the crystalline material [40]. In this case, the existence of a wide distribution of aggregates with different conformation and association degrees (size distribution) and the presence of weak interactions between the aggregates led also to an exotic spin glass magnetic behavior for this family of host–guest hybrid nanocomposite materials which is reminiscent of that of multidispersed superparamagnetic nanoparticles.

6. Multidimensional metal–organic polymers (MOPs): from low-dimensional (1D) single-chain to high-dimensional (2D and 3D) open-framework magnets

Heterobimetallic $M^{II}_nM'^{II}_m$ MOPs (M and M′ = Cu, Ni, Co, and Mn; n, $m = 1$–3) of varying dimensionality, ranging from one- (1D) to two- (2D) and three-dimensional (3D), have been rationally prepared starting from Cu^{II} (L = **1b**–**d**), M^{II}_2 (M = Cu, Ni, and Co; L = **2a**–**d**) and Cu^{II}_3 (L = **3a**) MOLs. In these cases, they act as bis-, tetrakis-, or hexakis-bidentate MOLs toward fully solvated M'^{II} ions (M′ = Co and Mn) with either water or dimethylsulfoxide (DMSO) as coordinating solvent (Table 3).

6.1. One-dimensional zigzag and linear MOPs

The $Cu^{II}M'^{II}$ 1D MOPs (M′ = Co and Mn; L = **1b**–**d**), with either zigzag or linear chain structures (Fig. 18a and b), behave as almost ideal ferrimagnetic chains [16,17]. In fact, the moderately strong antiferromagnetic coupling between the Cu^{II} and M'^{II} ions through the oxamato bridge ($J < 0$) is large enough to allow an important short-range intrachain magnetic correlation (Table 3).

Interestingly, the $Cu^{II}Co^{II}$ ferrimagnetic chains exhibit slow magnetic relaxation at low temperatures ($T_B < 3.5$ K) with an Arrhenius law dependence that is typical of the so-called single-chain magnets (SCMs) (Fig. 18c) [16,17]. As for the related SMM behavior, the SCM one has a pure dynamic origin which is associated with the Ising-type magnetic anisotropy of the isolated chain [42]. In fact, there is no long-range magnetic ordering at a finite temperature for 1D systems; this is expected to occur at absolute zero for a chain in lacking interchain interactions. Hence, this unprecedented SCM behavior for the family of oxamato-bridged heterobimetallic chains obeys the large intrachain Ising-type magnetic anisotropy and the minimization of the interchain interactions that result from the combination of an orbitally degenerate octahedral high-spin Co^{II} ion ($^4T_1$) and a square-planar Cu^{II} complex with sterically hindered polymethyl-substituted phenyl groups, respectively [16,17].

The aggregation of these $Cu^{II}M'^{II}$ ferrimagnetic chains into silica-based mesoporous materials has been recently achieved through a stepwise procedure involving the successive impregnation with the Cu^{II} MOL (L = **1c**) and M'^{II} ions (M′ = Co and Mn) [43]. The progressive aggregation of larger $[Cu^{II}Co^{II}]_n$ fragments of chains into the pores of the ordered mesoporous silica led to SCM behavior at low temperatures ($T_B < 2.0$ K), as for the crystalline material. This surface (heterogeneous) aggregation of SCMs may be an appealing alternative to the solution (heterogeneous) aggregation methods, as demonstrated earlier by some of us [44]. In fact, a slow magnetic relaxation below 6 K with an Arrhenius law dependence typical of genuine SCMs has been observed in a related oxamato-bridged $Cu^{II}Co^{II}$ ferrimagnetic chain which is built into porous Vycor glass (PVG). This new synthetic approach to prepare nanocomposite materials exhibiting slow magnetic relaxation will allow the control of the size-related magnetic properties at the nanometer scale. In this respect, the preparation of discrete chain fragments whose size is limited by the pore dimensions of the host silica support can provide new insights on the importance of finite-size effects in the mechanism of the slow relaxation of the magnetization in SCMs [42].

6.2. Two-dimensional brick-wall MOPs

On the contrary, the double *meta*-substituted phenylene linkers ensure a ferromagnetic interaction between the oxamato-bridged ferrimagnetic chains in the metallacyclophane-based $Cu^{II}_2M'^{II}_2$ 2D MOPs (M′ = Co and Mn; L = **2a**, **2b**, and **2d**) with a brick-wall layered structure (Fig. 19a) [45,46]. Hence, the $Cu^{II}_2Co^{II}_2$ 2D MOPs with the bulkier polymethyl-substituted ligands (L = **2b** and **2d**) show a long-range (most likely 2D) ferromagnetic order at $T_C = 5.0$ and 7.0 K because of the intralayer Ising-type magnetic anisotropy associated to the orbitally degenerate octahedral high-spin Co^{II} ion ($^4T_1$) and the minimization of the interlayer magnetic interactions (Fig. 19c) [46]. Indeed, long-range magnetic ordering is essentially a 3D phenomenon; however, long-range magnetic ordering may occur for a 2D system with an Ising-type magnetic anisotropy.

Instead, the $Cu^{II}_2Co^{II}_2$ 2D MOP with the less bulky ligand (L = **2a**) is a metamagnet with a long-range 3D antiferromagnetic ordering in zero-field at $T_N = 8.5$ K and a ferromagnetic-like transition at a critical field of 1.2 kOe (Fig. 19c) which is sufficient to overcome the weak interlayer antiferromagnetic interactions through the hydrogen-bonded crystallization water molecules (Fig. 19b) [45]. These results show how subtle differences in the packing of the layers influence dramatically

Table 3
Selected magnetic data for the MOPs.

Compound	d[a]	J[b] (cm^{-1})	D[c] (cm^{-1})	T_C[d] (K)	H_c[e] (Oe)	M_r[f] ($cm^3\ mol^{-1}$ Oe)	T_N[g] (K)	T_B[h] (K)	E_a[i] (cm^{-1})	τ_0[j] (s)	F[k]
Cu(**1b**)$_2$Mn(DMSO)$_2$	1D	−27.9									
Cu(**1c**)$_2$Mn(DMSO)$_2$	1D	−28.2									
Cu(**1d**)$_2$Mn(DMSO)$_2$·2DMSO	1D	−24.7									
Cu(**1b**)$_2$Co(DMSO)$_2$·DMSO	1D	−40.3	538								
Cu(**1c**)$_2$Co(DMSO)$_2$·DMSO	1D	−40.5	719					2.1			
Cu(**1d**)$_2$Co(DMSO)$_2$·DMSO	1D	−44.3	710					3.3	38.0	2.3×10^{-11}	0.25
Cu(**1c**)$_2$Co(H_2O)$_2$	1D	−45.8	692					<2.0			
Cu(**1d**)$_2$Co(H_2O)$_2$·4H_2O	1D	−35.0	610					2.2	16.3	4.0×10^{-9}	0.12
{[Cu$_2$(**2b**)$_2$][Mn(H_2O)$_2$]$_2$}·8H_2O	2D			13.5	50	5025					
{[Cu$_2$(**2d**)$_2$][Mn(H_2O)$_2$]$_2$}·8H_2O	2D			14.5	70	3215					
{[Cu$_2$(**2b**)$_2$][Mn(H_2O)$_2$]$_2$}	2D			<2.0							
{[Cu$_2$(**2d**)$_2$][Mn(H_2O)$_2$]$_2$}	2D			<2.0							
{[Cu$_2$(**2a**)$_2$][Co(H_2O)$_2$]$_2$}·8H_2O	2D						8.5				
{[Cu$_2$(**2b**)$_2$][Co(H_2O)$_2$]$_2$}·8H_2O	2D			5.0	475	760					
{[Cu$_2$(**2d**)$_2$][Co(H_2O)$_2$]$_2$}·8H_2O	2D			7.0	780	1565					
Li$_2${[Ni$_2$(**2a**)$_3$][Mn(H_2O)$_2$]$_3$}·22H_2O	3D			6.5	450	6200					
Li$_2${[Ni$_2$(**2c**)$_3$][Mn(H_2O)$_2$]$_3$}·25H_2O	3D			13.5	2250	11,100					
Li$_2${[Co$_2$(**2a**)$_3$][Mn(H_2O)$_2$]$_3$}·22H_2O	3D			6.5	175	1200					
Li$_2${[Co$_2$(**2c**)$_3$][Mn(H_2O)$_2$]$_3$}·21H_2O	3D			3.5	250	3500					
Li$_2${[Ni$_2$(**2a**)$_3$][Co(H_2O)$_2$]$_3$}·22H_2O	3D			5.5	465	1505					
Li$_2${[Ni$_2$(**2c**)$_3$][Co(H_2O)$_2$]$_3$}·20H_2O	3D			11.0	3750	2600					
Li$_2${[Ni$_2$(**2a**)$_3$][Mn(H_2O)$_2$]$_3$}	3D			8.0	200	780					
Li$_2${[Ni$_2$(**2a**)$_3$][Co(H_2O)$_2$]$_3$}	3D			6.5	300	1190					
Li$_2${[Co$_2$(**2a**)$_3$][Mn(H_2O)$_2$]$_3$}	3D			8.5	715	1020					
{[Cu$_3$(**3a**)$_2$][Mn(H_2O)$_2$]$_3$}·14H_2O	3D			28.0	55	1115					
{[Cu$_3$(**3a**)$_2$][Co(H_2O)$_2$]$_3$}·18H_2O	3D			14.0	2240	1720					

[a] d is the dimensionality.
[b] J is the exchange coupling parameter through the oxamato bridge [$\boldsymbol{H} = \sum_{i,j}(-J\boldsymbol{S}_{M,i}\boldsymbol{S}_{M',j} + D\boldsymbol{L}^2_{zM',j})$].
[c] D is the local axial magnetic anisotropy parameter [$\mathbf{H} = \sum_{i,j}(-J\mathbf{S}_{M,i}\mathbf{S}_{M',j} + D\mathbf{L}^{\mathbf{2}}_{zM',j})$].
[d] T_C is the Curie temperature corresponding to the long-range ferromagnetic ordering.
[e] H_c is the coercive field at T = 2.0 K.
[f] M_r is the remnant magnetization at T = 2.0 K.
[g] T_N is the Neel temperature corresponding to the long-range antiferromagnetic ordering.
[h] T_B is the blocking temperature calculated as the temperature of the maximum of χ''_M at ν = 1000 Hz ($T_B = T_{max}$).
[i] E_a is the activation energy for the magnetization reversal [$\tau = \tau_0\exp(E_a/k_BT)$].
[j] τ_0 is the preexponential factor [$\tau = \tau_0\exp(E_a/k_BT)$].
[k] F is the Mydosh parameter [$F = (\Delta T_{max}/T_{max})/\Delta(\log \nu)$].

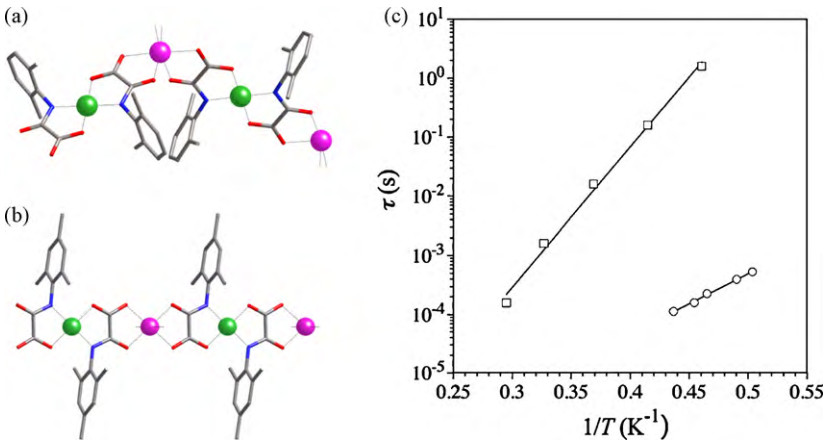

Fig. 18. Structures of the (a) zizzag and (b) linear neutral chains of Cu(**1c**)$_2$Co(H$_2$O)$_2$ and Cu(**1d**)$_2$Co(H$_2$O)$_2$·4H$_2$O, respectively. Ligand and metal atoms are represented by sticks and balls, respectively (C, gray; N, blue; O, red; Cu, green; Co, purple). (c) Arrhenius plots for Cu(**1d**)$_2$Co(H$_2$O)$_2$·4H$_2$O (○) and Cu(**1d**)$_2$Co(DMSO)$_2$·DMSO (□). The solid lines are the best-fit curves (see Table 3).

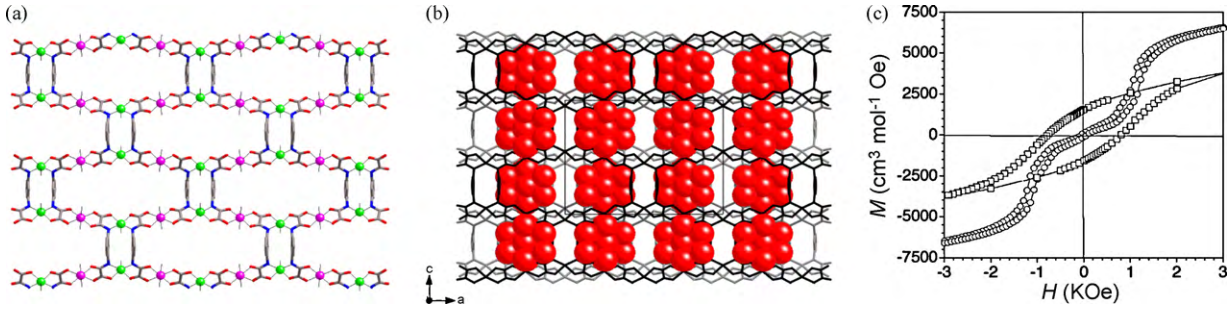

Fig. 19. (a) Structure of a brick-wall neutral layer and (b) crystal packing of the layers of {[Cu$_2$(**2a**)$_2$][Co(H$_2$O)$_2$]$_2$}·8H$_2$O. Ligand and metal atoms are represented by sticks and balls respectively (C, gray; N, blue; O, red; Cu, green; Co, purple), while the oxygen atoms from coordinated and crystallization water molecules are represented by red spheres. (c) Magnetization hysteresis loops at 2.0 K for {[Cu$_2$(**2a**)$_2$][Co(H$_2$O)$_2$]$_2$}·8H$_2$O (○) and {[Cu$_2$(**2d**)$_2$][Co(H$_2$O)$_2$]$_2$} · 8H$_2$O (□).

the 3D magnetic behavior and, at the same time, they underline the limits of the 2D strategy to obtain molecule-based magnets because of the difficulty to control the interlayer interactions.

So, the related $Cu^{II}_2Mn^{II}_2$ 2D MOPs (L = **2b** and **2d**) show long-range 3D ferromagnetic order at higher critical temperatures (T_C = 13.5 and 14.5 K) than their $Cu^{II}_2Co^{II}_2$ homologues (Table 3) [46]. In this case, the observation of a long-range 2D ferromagnetic order is precluded because of the magnetically isotropic nature of the octahedral high-spin Mn^{II} ion with no first-order orbital contribution ($^6A_1$). Thus, the dehydrated derivatives of these $Cu^{II}_2Mn^{II}_2$ 2D MOPs show no long-range magnetic order above 2.0 K independently of the nature of the polymethyl-substituted ligand (L = **2b** and **2d**) (Table 3) [46]. This fact points to the importance of the weak interlayer ferromagnetic interactions through the hydrogen-bonded crystallization water molecules in the long-range 3D ferromagnetic order of the parent hydrated $Cu^{II}_2Mn^{II}_2$ 2D MOPs (Fig. 19b).

Overall, these results show the need to increase the dimensionality in order to obtain high-T_C molecule-based magnets. On the other hand, in terms of future applications of these molecular magnetic materials, the coercivity that confers a memory effect to the material is as important as the critical temperature. Thus, the $Cu^{II}_2Mn^{II}_2$ 2D MOPs are soft magnets (H_c = 50–70 Oe) whereas the $Cu^{II}_2Co^{II}_2$ homologues are hard magnets (H_c = 475–780 Oe) (Table 3), the observed differences in coercivity being likely related to the distinct local magnetic anisotropy of the M'^{II} ions (M = Mn and Co) [46].

6.3. Three-dimensional hexagonal diamond MOPs

The metallacryptand-based $M^{II}_2M'^{II}_3$ 3D MOPs (M = Ni and Co; M′ = Co and Mn; L = **2a** and **2c**) would possess a hexagonal diamond network structure similar to that of their $M^{II}_2Li^{I}_3$ analogues (Fig. 20a) [47,48]. In this case, the triple *meta*-substituted phenylene linkers ensure a ferromagnetic interaction between the oxamato-bridged ferrimagnetic planes that leads to a long-range 3D ferromagnetic order at T_C = 3.5–13.5 K (Fig. 20c) [47,48]. Moreover, the coercivity is relatively large in these $M^{II}_2M'^{II}_3$ 3D MOPs (H_c = 175–3750 Oe) (Table 3), as expected from the moderate to strong local magnetic anisotropy of the M^{II} ions (M = Ni and Co). They represent thus the first examples of oxamato-bridged heterobimetallic molecule-based magnets based on 3D MOPs. In fact, a large number of oxamato-bridged heterobimetallic 1D and 2D MOPs that order ferromagnetically through interchain and interplanar interactions, respectively, were earlier reported by Kahn and coworkers [11].

On the other hand, this family of molecule-based magnets with an open-framework structure, referred to as open-framework magnets (OFMs), are ideal candidates to obtain multifunctional materials [49]. In fact, the anionic $M^{II}_2M'^{II}_3$ 3D MOPs host a large amount of crystallization water molecules and hydrated Li^{I} countercations, which are either weakly bound to the host surface or form discrete chains aligned in the hexagonal channels (Fig. 20b) [47,48]. Indeed, one could envisage to remove the crystallization water molecules leaving unaltered their open-framework structure and readily available to selectively adsorb other small solvent (MeOH, EtOH, or PrOH) or gas (N_2, H_2, CH_4, CO, or CO_2) molecules.

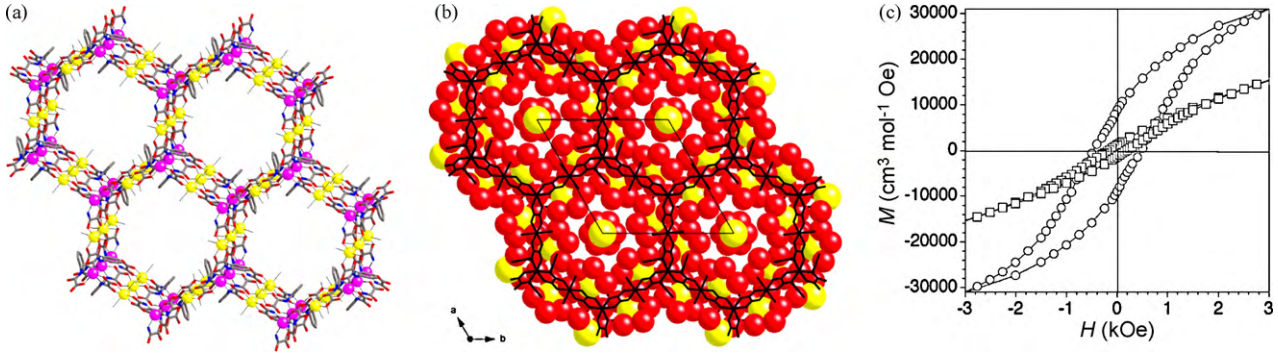

Fig. 20. (a) Structure of the hexagonal diamond anionic network and (b) crystal packing of the solvated alkaline countercations of $Li_5\{[M_2(\mathbf{2a})_3][Li(H_2O)_2]_3\}\cdot 31H_2O$ (M = Ni and Co). Ligand and metal atoms are represented by sticks and balls, respectively (C, gray; N, blue; O, red; Li, yellow; M, purple), while the lithium atoms from solvated alkaline countercations and the oxygen atoms from coordinated and crystallization water molecules are represented by yellow and red spheres, respectively. (c) Magnetization hysteresis loops at 2.0 K for $Li_2\{[Ni_2(\mathbf{2a})_3][Mn(H_2O)_2]_3\}\cdot 22H_2O$ (○) and $Li_2\{[Ni_2(\mathbf{2a})_3][Co(H_2O)_2]_3\}\cdot 22H_2O$ (□).

At this regard, the small variation of the T_C values from 5.5 and 6.5 up to 8.0 and 8.5 K for the $Ni^{II}{}_2M^{II}{}_3$ 3D MOPs (M = Mn and Co, respectively) as a function of the water contents (solvatomagnetic effects) underlines their potential use as magnetic sensors (Table 3). However, the presence of counterbalancing Li^I ions as hosts within the pore system of the anionic open-framework structure accounts for its limited sorption capacity toward solvent molecules and gases [47].

Having this in mind, we have prepared triangular metallacyclophane-based $Cu^{II}{}_3M'^{II}{}_3$ 3D MOPs (M′ = Co and Mn; L = **3a**) with a putative trigonal open-framework structure (Fig. 4d) [50]. Our preliminary results show a long-range 3D ferromagnetic order at T_C = 14.0 and 28.0 K depending on the nature of the M'^{II} ion (M′ = Co and Mn, respectively) (Table 3). Future work will focus on the study of the sorption properties of these neutral $Cu^{II}{}_3M'^{II}{}_3$ 3D MOPs in order to get the first examples of oxalamide-based porous magnets for future applications in gas storage and transport and host–guest magnetic sensing [49].

7. Conclusions and outlook: toward metallosupramolecular multifunctional materials

In this review, the supramolecular coordination chemistry of aromatic polyoxalamide (APOXA) ligands with paramagnetic 3d metal ions has been outlined. The ligand design strategy has led to oligonuclear metal complexes that can behave as effective molecular magnetic wires (MMWs) and molecular magnetic switches (MMSs) for the transmission of electron exchange interactions. Moreover, they have been used as metal–organic ligands (MOLs) for the preparation of high-nuclearity metal–organic clusters (MOCs) and high-dimensionality metal–organic polymers (MOPs) with interesting magnetic properties. As a matter of fact, this strategy has provided the first examples of oxamato-bridged single-molecule magnets (SMMs) and single-chain magnets (SCMs), and it has also allowed the entry to oxamato-bridged open-framework magnets (OFMs). This new family of oxalamide-based, low- (0D and 1D) and high-dimensional (2D and 3D) magnets exemplifies thus the current trends and the future challenges in the metallosupramolecular approach to functional magnetic materials.

Having this in mind, we are currently expanding this metallosupramolecular approach to the synthesis of multifunctional magnetic materials displaying unique magnetic properties as well as redox, optical, sensor, or catalytic activities. In fact, the great flexibility and versatility of metallosupramolecular chemistry offer the possibility to associate different properties in the same material, which can function either in independent or concerted (synergic) ways. This is a major current challenge in materials science and nanotechnology that requires the collaboration of groups from different disciplines, including both organic and inorganic chemists, theoretical chemists and physicists. Doubtless, this is the more attractive part of this approach and the main reason for us to pursue in this research avenue.

Acknowledgements

This work was supported by theMFR and the CNRS (France), the CAPES (Brazil) (Project COFECUB 460/04), the MICINN (Spain) (Projects CTQ2007-61690, CSD2006-00015 CSD2007-00010, and MAT2007-60660), the Generalitat Valenciana (Spain) (Project PROMETEO/2009/108), the Gobierno Autónomo de Canarias (Spain) (Project PI2002/175), the Agencia Canaría de Investigación, Innovación y Sociedad de la Información (Spain) (Project SolSubC200801000389) and the European Union through the Magmanet Network of Excellence (Contract 03/197).

References

[1] J.M. Lehn, Supramolecular Chemistry: Concepts and Perspectives, VCH, Weinheim, 1995.
[2] (a) M.C. Etter, Acc. Chem. Res. 23 (1990) 120;
(b) C.B. Aakeröy, K.R. Seddon, Chem. Soc. Rev. 22 (1993) 397;
(c) G.R. Desiraju, Angew. Chem. Int. Ed. Engl. 34 (1995) 2311;
(d) G.M. Whitesides, E.E. Simanek, J.P. Mathias, C.T. Seto, D.N. Chin, M. Mammen, D.M. Gordon, Acc. Chem. Res. 28 (1995) 37;
(e) J. Rebek Jr., Chem. Soc. Rev. 25 (1996) 255.
[3] (a) E.C. Constable, Prog. Inorg. Chem. 42 (1994) 67;
(b) P.J. Stang, B. Olenyuk, Acc. Chem. Res. 30 (1997) 502;
(c) M. Albrecht, Chem. Soc. Rev. 27 (1998) 281;
(d) G.F. Swiegers, T.J. Malefetse, Chem. Rev. 100 (2000) 3483;
(e) P.J. Steel, Acc. Chem. Res. 38 (2005) 243.
[4] (a) M. Fujita, Chem. Soc. Rev. 27 (1998) 417;
(b) D.L. Caulder, K.N. Raymond, Acc. Chem. Res. 32 (1999) 975;
(c) S. Lenninger, B. Olenyuk, J. Stang, Chem. Rev. 100 (2000) 853;
(d) S.R. Seidel, P.J. Stang, Acc. Chem. Res. 35 (2002) 972.
[5] (a) S.R. Batten, R. Robson, Angew. Chem. Int. Ed. 37 (1998) 1461;
(b) F.A. Cotton, C. Lin, C.A. Murillo, Proc. Natl. Acad. Sci. 99 (2002) 4810;
(c) O.M. Yaghi, M. O'Keeffe, N.W. Ockwig, H.K. Chae, M. Eddaoudi, J. Kim, Nature 423 (2003) 705;
(d) G. Férey, C. Mellot-Draznieks, C. Serre, F. Millange, Acc. Chem. Res. 38 (2005) 217.
[6] (a) D. Fiedler, D.H. Leung, R.G. Bergman, K.N. Raymond, Acc. Chem. Res. 38 (2005) 349;
(b) M.P. Suh, Y.E. Cheon, E.Y. Lee, Coord. Chem. Rev. 252 (2008) 1007;
(c) D. Farruseng, S. Aguado, C. Pinel, Angew. Chem. Int. Ed. 48 (2009) 7502;
(d) R.J. Kuppler, D.J. Timmons, Q.R. Fang, J.R. Li, T.A. Makal, M.D. Young, D. Yuan, D. Zhao, W. Zhuang, H.C. Zhou, Coord. Chem. Rev. 253 (2009) 3042.
[7] (a) J.M. Lehn, Angew. Chem. Int. Ed. 43 (2004) 3644;
(b) L.K. Thompson, O. Waldman, Coord. Chem. Rev. 249 (2005) 2677;
(c) M. Kurmoo, Chem. Soc. Rev. 38 (2008) 1353;
(d) L.R. MacGillivray, G.S. Papaefstathiou, T. Friscic, T.D. Hamilton, D.K. Buar, Q. Chu, D.B. Varshney, I.G. Georgiev, Acc. Chem. Res. 41 (2008) 280.

[8] (a) O. Kahn, Molecular Magnetism, VCH, New York, 1993;
(b) O. Kahn (Ed.), Magnetism: A Supramolecular Function (NATO ASI Series C), vol. 484, Kluwer, Dordrecht, 1996;
(c) Coord. Chem. Rev. 249 (2005) 2677;
(d) Aust. J. Chem. 62 (2009) 1079.
[9] (a) M. Verdaguer, A. Bleuzen, V. Marvaud, J. Vaissermann, M. Seuleiman, C. Desplanches, A. Scuiller, C. Train, R. Garde, G. Gelly, C. Lomenech, I. Rosenman, P. Veillet, C. Cartier, F. Villain, Coord. Chem. Rev. 190–192 (1999) 1023;
(b) M. Ohba, H. Okawa, Coord. Chem. Rev. 198 (2000) 313;
(c) V. Marvaud, J.M. Herrera, T. Barilero, F. Tuyèras, R. Garde, A. Scuiller, C. Decroix, M. Cantuel, C. Desplanches, Monatsh. Chem. 134 (2003) 149;
(d) L.M.C. Beltran, J.R. Long, Acc. Chem. Res. 38 (2005) 325;
(e) R. Lescouëzec, L.M. Toma, J. Vaissermann, M. Verdaguer, F.S. Delgado, C. Ruiz-Pérez, F. Lloret, M. Julve, Coord. Chem. Rev. 249 (2005) 2691.
[10] (a) S. Decurtins, R. Pellaux, G. Antorrena, F. Palacio, Coord. Chem. Rev. 190–192 (1999) 841;
(b) E. Coronado, M. Clemente-León, J.R. Galán-Mascaros, C. Giménez-Saiz, C.J. Gómez-García, E. Martínez-Ferrero, J. Chem. Soc., Dalton Trans. (2000) 3955;
(c) M. Pilkington, M. Gross, P. Franz, M. Biner, S. Decurtins, H. Stoeckli-Evans, A. Neels, J. Sol. State Chem. 159 (2001) 262;
(d) E. Coronado, A. Forment-Aliaga, J.R. Galán-Mascaros, C. Giménez-Saiz, C.J. Gómez-García, E. Martínez-Ferrero, A. Nuez, F.M. Romero, Solid State Sci. 5 (2003) 917;
(e) M. Gruselle, C. Train, K. Boubekeur, P. Gredin, N. Ovanesyan, Coord. Chem. Rev. 250 (2006) 2491.
[11] (a) O. Kahn, Struct. Bond. 68 (1987) 89;
(b) O. Kahn, Acc. Chem. Res. 33 (2000) 647.
[12] (a) Y. Journaux, R. Ruiz, A. Aukauloo, Y. Pei, Mol. Cryst. Liq. Cryst. 305 (1997) 193;
(b) R. Ruiz, J. Faus, F. Lloret, M. Julve, Y. Journaux, Coord. Chem. Rev. 193–195 (1999) 1069;
(c) E. Pardo, R. Ruiz-García, J. Cano, X. Ottenwaelder, R. Lescouëzec, Y. Journaux, F. Lloret, M. Julve, Dalton Trans. (2008) 2780.
[13] (a) J.S. Miller, A.J. Epstein, Angew. Chem. Int. Ed. Engl. 33 (1994) 385;
(b) O. Kahn, Adv. Inorg. Chem. 43 (1995) 179;
(c) W. Linert, M. Verdaguer, Molecular Magnets. Recent Highlights, Springer Verlag, 2003.
[14] G. Blay, I. Fernández, J.R. Pedro, R. Ruiz-García, M.C. Muñoz, J. Cano, R. Carrasco, Eur. J. Org. Chem. (2003) 1627.
[15] M.C. Muñoz, G. Blay, I. Fernández, J.R. Pedro, R. Carrasco, R. Ruiz-García, J. Cano, submitted for publication.
[16] E. Pardo, R. Ruiz-García, F. Lloret, J. Faus, M. Julve, Y. Journaux, F.S. Delgado, C. Ruiz-Pérez, Adv. Mater. 16 (2004) 1597.
[17] E. Pardo, R. Ruiz-García, F. Lloret, J. Faus, M. Julve, Y. Journaux, M.A. Novak, F.S. Delgado, C. Ruiz-Pérez, Chem. Eur. J. 13 (2007) 2054.
[18] I. Fernández, R. Ruiz, J. Faus, M. Julve, F. Lloret, J. Cano, X. Ottenwaelder, Y. Journaux, M.C. Muñoz, Angew. Chem. Int. Ed. 40 (2001) 3039.
[19] E. Pardo, J. Faus, M. Julve, F. Lloret, M.C. Muñoz, J. Cano, X. Ottenwaelder, Y. Journaux, R. Carrasco, G. Blay, I. Fernández, R. Ruiz-García, J. Am. Chem. Soc. 125 (2003) 10770.
[20] J.A. McCleverty, M.D. Ward, Acc. Chem. Res. 31 (1998) 842.
[21] E. Pardo, M.C. Dul, R. Lescouëzec, Y. Journaux, J. Ferrando-Soria, R. Ruiz-García, J. Cano, L. Cañadillas-Delgado, J. Pasán, C. Ruiz-Pérez, M. Julve, F. Lloret, in preparation.
[22] (a) H. Iwamura, N. Koga, Acc. Chem. Res. 26 (1993) 346;
(b) A. Rajca, Chem. Rev. 94 (1994) 871.
[23] E. Pardo, M.C. Dul, D. Cangussu, R. Lezcouëzec, L.M. Chamoreau, Y. Journaux, R. Ruiz-García, J. Cano, M. Julve, F. Lloret, O. Fabelo, J. Pasán, C. Ruiz-Pérez, in preparation.
[24] (a) T. Glaser, M. Gerenkamp, R. Fröhlich, Angew. Chem. Int. Ed. 41 (2002) 3823;
(b) T. Glaser, M. Heidemeier, J.B.H. Strautmann, H. Bögge, A. Stammler, E. Krickemeyer, R. Huenerbein, S. Grimme, E. Bothe, E. Bill, Chem. Eur. J. 13 (2007) 9191.
[25] M.C. Dul, E. Pardo, R. Lezcouëzec, L.M. Chamoreau, F. Villain, Y. Journaux, R. Ruiz-García, J. Cano, M. Julve, F. Lloret, J. Pasán, C. Ruiz-Pérez, J. Am. Chem. Soc. 131 (2009) 14614.
[26] M.C. Dul, X. Ottenwaelder, E. Pardo, R. Lezcouëzec, Y. Journaux, L.M. Chamoreau, R. Ruiz-García, J. Cano, M. Julve, F. Lloret, Inorg. Chem. 48 (2009) 5244.
[27] (a) J.F. Berry, F.A. Cotton, L.M. Daniels, C.A. Murillo, J. Am. Chem. Soc. 124 (2002) 3212;
(b) S.Y. Lin, I.W.P. Chen, C.H. Chen, M.H. Hsieh, C.Y. Yeh, T.W. Lin, Y.H. Chen, S.M.J. Peng, Phys. Chem. B 108 (2004) 959.
[28] E. Pardo, K. Bernot, M. Julve, F. Lloret, J. Cano, R. Ruiz-García, F.S. Delgado, C. Ruiz-Pérez, X. Ottenwaelder, Y. Journaux, Inorg. Chem. 43 (2004) 2768.
[29] E. Pardo, R. Ruiz-García, F. Lloret, M. Julve, J. Cano, J. Pasán, C. Ruiz-Pérez, Y. Filali, L.M. Chamoreau, Y. Journaux, Inorg. Chem. 46 (2007) 4504.
[30] D.A. Dougherty, Acc. Chem. Res. 24 (1991) 88.
[31] E. Pardo, K. Bernot, M. Julve, F. Lloret, J. Cano, R. Ruiz-García, J. Pasán, C. Ruiz-Pérez, X. Ottenwaelder, Y. Journaux, Chem. Commun. (2004) 920.
[32] E. Pardo, M.C. Dul, R. Lescouëzec, L.M. Chamoreau, Y. Journaux, J. Pasán, C. Ruiz-Pérez, M. Julve, F. Lloret, R. Ruiz-García, J. Cano, Dalton Trans. (2010), doi:10.1039/b926709c.
[33] E. Pardo, I. Morales-Osorio, M. Julve, F. Lloret, J. Cano, R. Ruiz-García, J. Pasán, C. Ruiz-Pérez, X. Ottenwaelder, Y. Journaux, Inorg. Chem. 43 (2004) 7594.
[34] X. Ottenwaelder, J. Cano, Y. Journaux, E. Rivière, C. Brennan, M. Nierlich, R. Ruiz-García, Angew. Chem. Int. Ed. 43 (2004) 850.
[35] M.C. Dul, E. Pardo, R. Lezcouëzec, Y. Journaux, O. Fabelo, J. Pasán, C. Ruiz-Pérez, J. Ferrando-Soria, R. Ruiz-García, J. Cano, M. Julve, F. Lloret, in preparation.
[36] (a) R.E.P. Winpenny, Angew. Chem. Int. Ed. 47 (2008) 7992;
(b) G.A. Timco, F. Troiani, F. Tuna, R.J. Pritchard, C.A. Muryn, E.J.L. McInnes, A. Guirri, A. Candini, P. Santini, G. Amoretti, M. Afronte, R.E.P. Winpenny, Nat. Nanotechnol. 4 (2009) 173.
[37] (a) D. Gatteschi, R. Sessoli, Angew. Chem. Int. Ed. 42 (2003) 268;
(b) D. Gatteschi, R. Sessoli, J. Villain, Molecular Nanomagnets, Oxford University Press, 2006.
[38] (a) J.A. Mydosh, Spin Glasses: An Experimental Introduction, Taylor & Francis, London, 1993;
(b) D. Chowdhury, Spin Glasses and Other Frustrated Systems, Princeton University Press, New Jersey, 1986.
[39] (a) M. Ruben, J.M. Lehn, P. Müller, Chem. Soc. Rev. 35 (2006) 1056;
(b) L.N. Dawe, K.V. Shuvaev, L.K. Thompson, Inorg. Chem. 48 (2009) 3323;
(c) D. Gatteschi, A. Cornia, M. Maninni, R. Sessoli, Inorg. Chem. 48 (2009) 3408.
[40] E. Pardo, P. Burguete, R. Ruiz-García, M. Julve, D. Beltrán, Y. Journaux, P. Amorós, F. Lloret, J. Mater. Chem. 16 (2006) 270.
[41] L. Toma, M.C. Dul, E. Pardo, R. Ruiz-García, M. Julve, Y. Journaux, F. Lloret, in preparation.
[42] (a) C. Coulon, H. Miyasaka, R. Clérac, Struct. Bond. 122 (2006) 163;
(b) H. Miyasaka, M. Julve, M. Yamashita, R. Clérac, Inorg. Chem. 48 (2009) 3420.
[43] D. Cangussu, J. El Haskouri, E. Pardo, R. Ruiz-García, M. Julve, D. Beltrán, Y. Journaux, P. Amorós, F. Lloret, in preparation.
[44] D. Cangussu, W.C. Nunes, C.L.M. Pereira, E.F. Pedroso, I.O. Mazali, M. Knobel, O.L. Alves, H.O. Stumpf, Eur. J. Inorg. Chem. (2008) 3802.
[45] C.L.M. Pereira, E.F. Pedroso, H.O. Stumpf, M.A. Novak, L. Ricard, R. Ruiz-García, E. Rivière, Y. Journaux, Angew. Chem. Int. Ed. 43 (2004) 956.
[46] J. Ferrando-Soria, E. Pardo, R. Ruiz-García, M. Julve, F. Lloret, M.C. Dul, R. Lezcouëzec, Y. Journaux, O. Fabelo, J. Pasán, C. Ruiz-Pérez, in preparation.
[47] E. Pardo, D. Cangussu, M.C. Dul, R. Lescouëzec, P. Herson, Y. Journaux, E.F. Pedroso, C.L.M. Pereira, M.C. Muñoz, R. Ruiz-García, J. Cano, P. Amorós, M. Julve, F. Lloret, Angew. Chem. Int. Ed. 47 (2008) 4211.
[48] D. Cangussu, E. Pardo, M.C. Dul, R. Lescouëzec, P. Herson, Y. Journaux, E.F. Pedroso, C.L.M. Pereira, H.O. Stumpf, M.C. Muñoz, R. Ruiz-García, J. Cano, M. Julve, F. Lloret, Inorg. Chim. Acta 361 (2008) 3394.
[49] D. Maspoch, D. Ruiz-Molina, J. Veciana, Chem. Soc. Rev. 36 (2007) 770.
[50] M.C. Dul, E. Pardo, R. Lezcouëzec, Y. Journaux, R. Ruiz-García, M. Julve, F. Lloret, in preparation.